Supplementary Material

Ab-initio Molecular Dynamics Simulation of Condensed-Phase Reactivity: The Electrolysis of Ammonia and Ethanimine Aqueous Solutions with Dissolved Carbon Dioxide

Contents

The Supplementary Material contains the complete evaluation of all systems investigated (pages 1 – 21), the list of educts, products and intermediates (page 22), the method comparison (pages 24 – 27), and the resulting structures (pages 27 – 32).

Methods

Car–Parrinello molecular dynamics simulations using the CPMD code[1,2] have been performed using the Becke–Lee–Yang–Parr (BLYP)[3,4] functional in connection with the Grimme dispersion correction[5]. The time step was chosen as 2 a.u. (0.048 fs) and the fictitious electron mass as 200 a.u. Troullier–Martins pseudopotentials as optimized for the BLYP functional were employed for describing the core electrons[6,7]. The plane-wave cutoff, which determines the size of the basis set, was set to 70.0 Rydberg. The simulation cells were 20 × 20 × 20 a.u.^{3} (10.6 ×10.6 ×10.6 Å^3). Solutions with a density of roughly 1.22 g/cm^3 were generated (8 ammonia, 9 carbon dioxide and 19 water molecules named **System 1** or 7 ammonia, 9 carbon dioxide and 19 water molecules named **System 2**). Density of the created solutions is higher than that of pure water (1.00 g/cm^3) because several water molecules are substituted with CO_2, which has higher molecular weight. After equilibration of stable, neutral, closed-shell systems, reactive species were generated in two ways: by removing eight hydrogen radicals, leading to OH radicals in order to simulate anodic conditions and by removing eight OH radicals, leading to eight hydrogen radicals in order to simulate cathodic conditions. For the reactive simulations, the spin-unrestricted version of Kohn–Sham theory was employed[8].

Results and discussion

The most complex and important processes were observed during simulations of anodic conditions, that is why it makes more sense to begin the discussion with their detailed description. In order to better simulate the real systems, two new cells were created for each neutral equilibrated system, which differed only in the positions of created OH radicals. As expected, the formation of various reactive oxygen-based species was observed (e.g., hydrogen peroxide HOOH, HOO radical, O_2). Furthermore, ammonia molecules were oxidized to several inorganic compounds, such as NHO, NO, NH_2OH, NH_2O, and NH_2.

NHO formation mechanism in **System 1**:

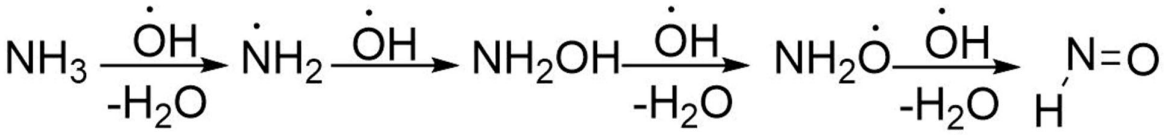


Figure S*1*. Sequence of elementary reaction steps that lead to the formation of HNO molecule in **System 1**.

The first reaction step corresponds to the abstraction of hydrogen radical from ammonia by OH radical which results in the formation of NH_2 radical after 0.16 ps of simulation. The formed reactive intermediate is attacked further by second OH radical in 0.02 ps. As a result the stable closed-shell hydroxylamine is formed. Key bond lengths for first and second reaction steps are depicted in **Figure *S*2** . Afterwards the hydrogen atom of the hydroxyl group is attacked by third equivalent of OH radical and results in the formation of NH_2O radical and water molecule. The new reactive intermediate is stabilized during the last step of the reaction via hydrogen radical abstraction, which is performed by the fourth equivalent of OH radical. The closed-shell stable HNO molecule is formed after 0.35 ps. The second and fourth reaction steps are much slower than hydrogen radical abstractions, that is why they should be considered as rate determining steps. Key bond lengths for third and fourth reaction steps are depicted in **Figure *S*3**.

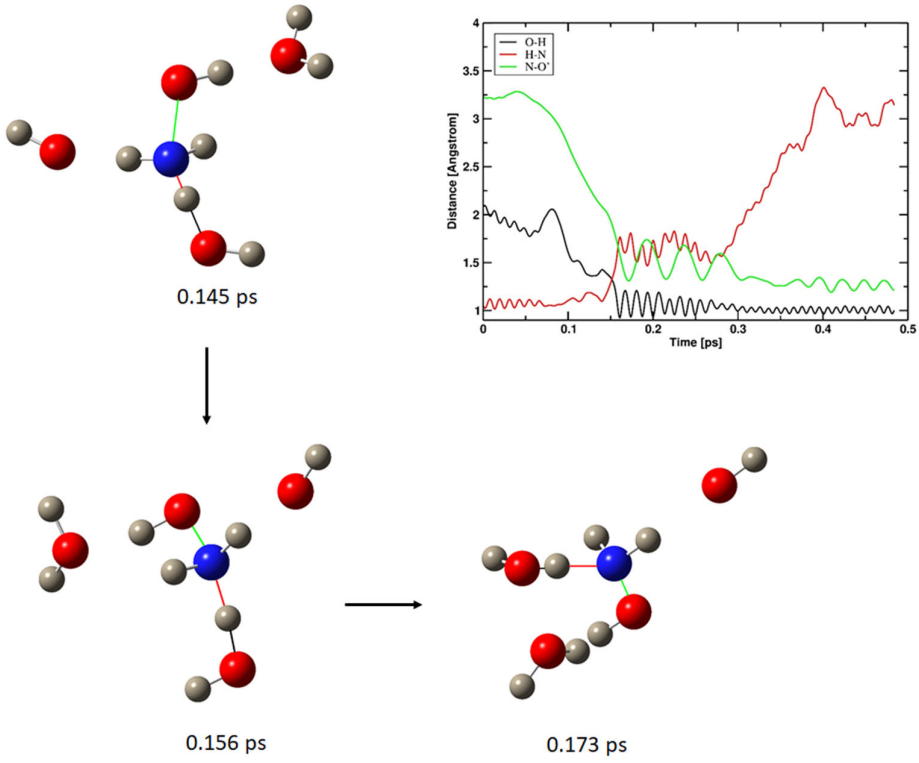


Figure S*2*. Sketch of the first and second reaction steps of ammonia with OH radicals. The most relevant bonding interactions deduced from Car-Parrinello simulations are highlighted.

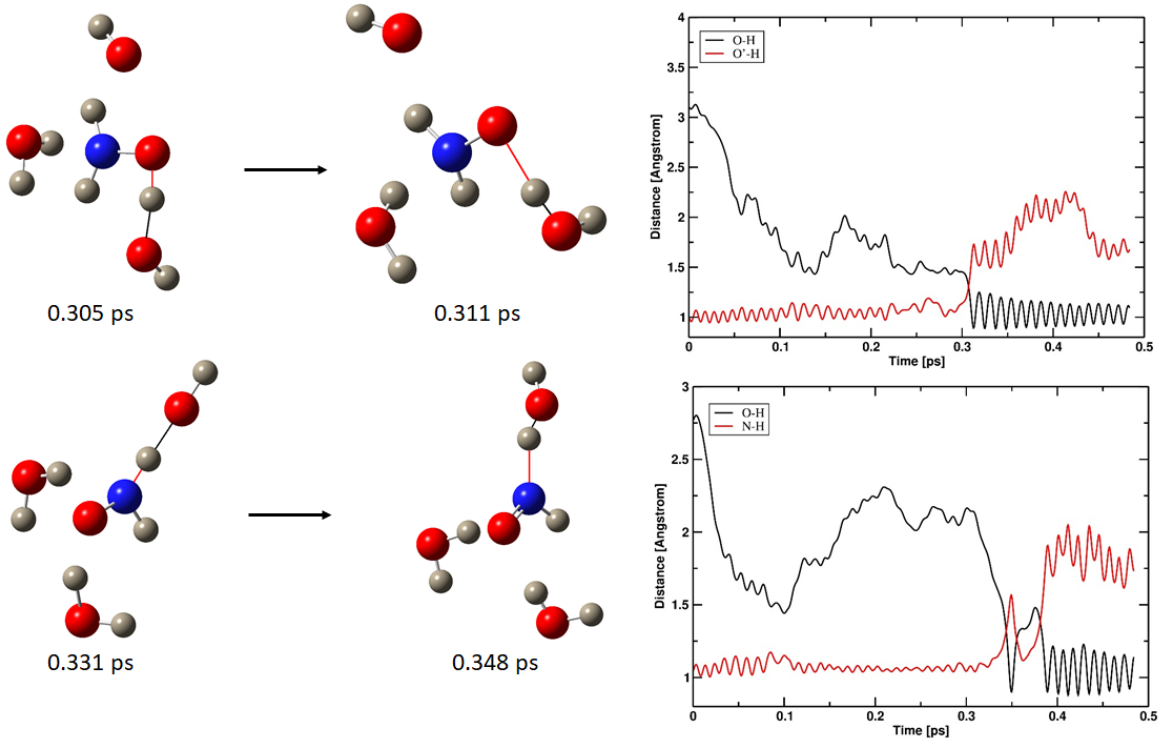


Figure S*3*. Sketch of the third and fourth reaction steps of ammonia with OH radicals. The most relevant bonding interactions deduced from Car-Parrinello simulations are highlighted.

NO formation mechanism 1 in **System 1**:

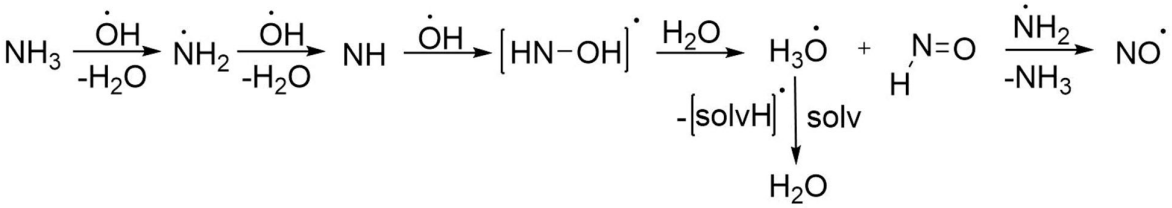


Figure S*4***.** Sequence of elementary reaction steps that lead to the formation of NO molecule in **System 1**.

The first reaction step corresponds to the abstraction of hydrogen radical from ammonia by OH radical which results in the formation of NH_2 radical after 0.16 ps of simulation. The formed reactive intermediate is attacked further by second OH radical in less than 0.01 ps resulting in the formation of NH intermediate. During the third step nitrene intermediate NH reacts with second equivalent of OH radical yielding HNOH intermediate, which is subsequently stabilized by abstraction of hydrogen atom by third equivalent of OH radical. Key bond lengths for first and second reaction steps are depicted in **Figure *S***5. Third reaction step lasts 0.06 ps and ends after 0.22 ps of simulation. The last step correspond to the abstraction of hydrogen atom by NH_2 radical, which yields NO and NH_3 molecules. From the figures below it is obvious that third step is the slowest one and thus should be considered as rate determining one. The process of NO formation takes 0.23 ps according to Car-Parrinello MD simulation. Key bond lengths for third and fourth

reaction steps are depicted in **Figure *S*6** . The initial temperature of the system in this case was set to 250 K.

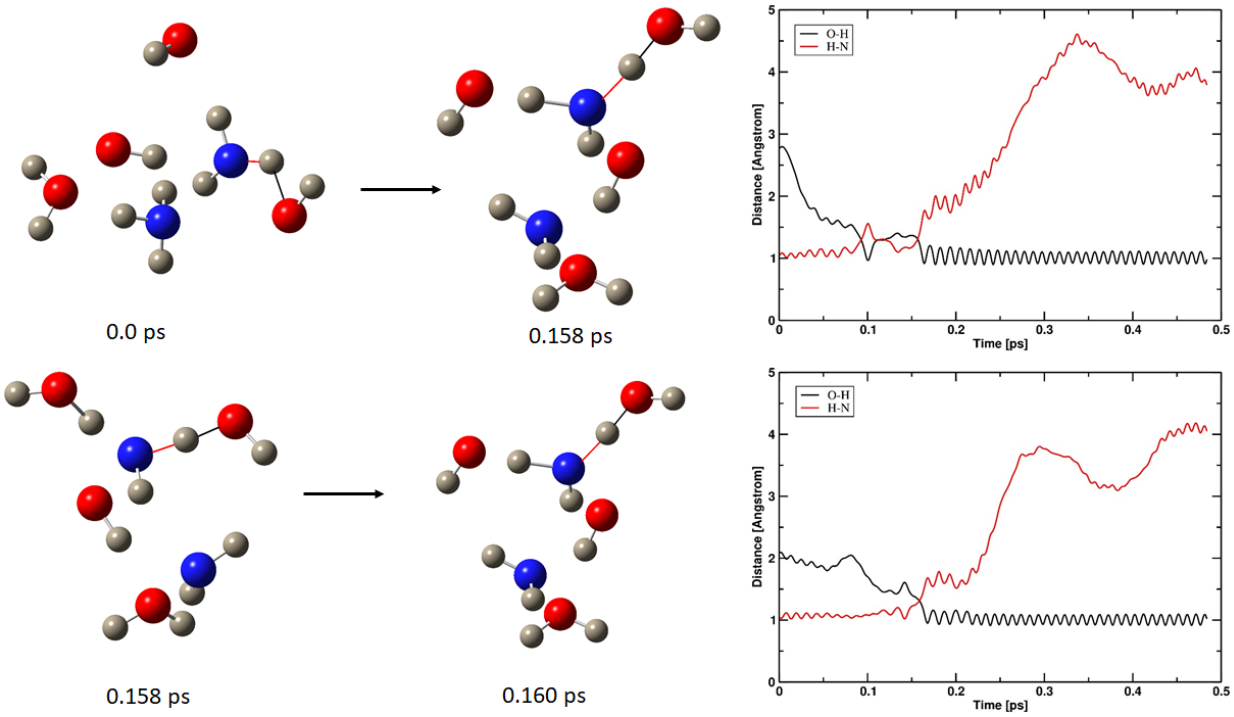


Figure S*5*. Sketch of the first and second reaction steps of ammonia with OH and NH_2 radicals. The most relevant bonding interactions deduced from Car-Parrinello simulations are highlighted.

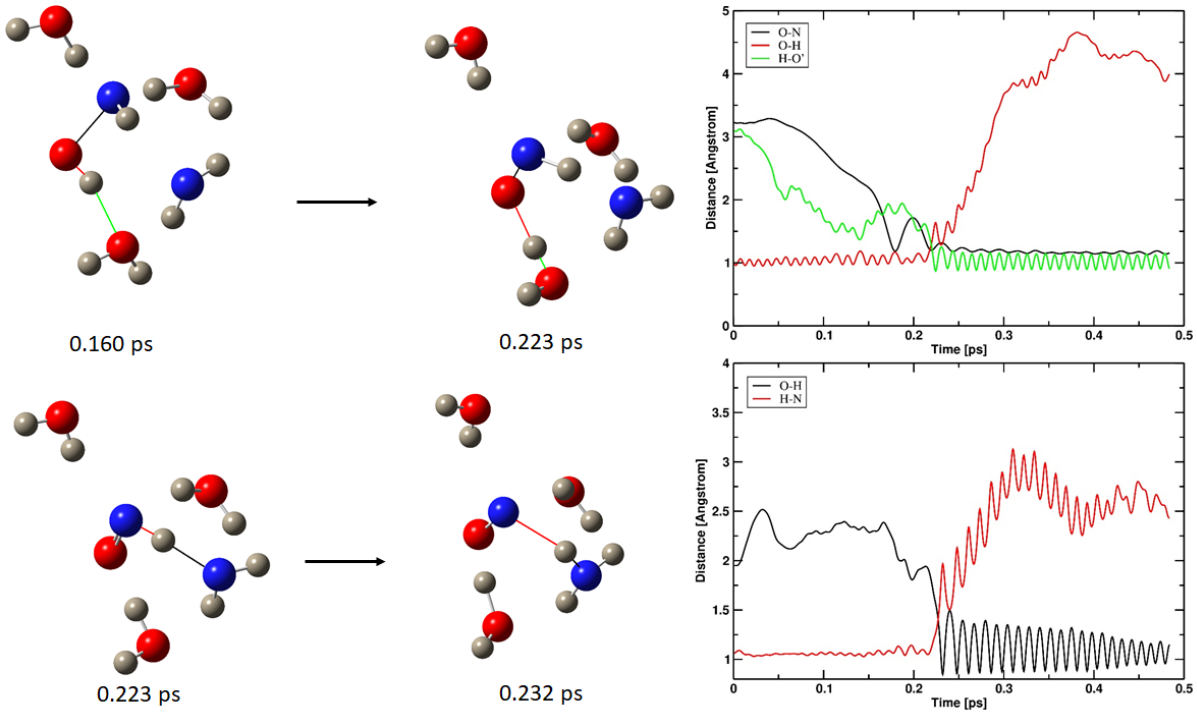


Figure S*6*. Sketch of the third and fourth reaction steps of ammonia with OH and NH_2 radicals. The most relevant bonding interactions deduced from Car-Parrinello simulations are highlighted.

NO formation mechanism 2 in **System 1**:

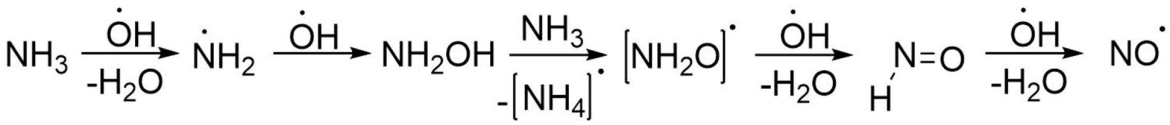


Figure S7. Second sequence of elementary reaction steps that lead to the formation of NO molecule in **System 1**.

The first reaction step corresponds to the abstraction of hydrogen radical from ammonia by OH radical which results in the formation of NH_2 radical after 0.06 ps of simulation. The formed reactive intermediate is attacked further by second OH radical in 0.05 ps resulting in the formation of NH_2OH intermediate. Key bond lengths for first and second reaction steps are depicted in **Figure *S*8**. During the third step hydroxylamine reacts with second equivalent of NH_3 yielding NH2O radical intermediate and neutral ammonium radical after 0.14 ps of simulation. The first one reacts further with OH radical resulting in the formation of water molecule and and closed shell HNO. The last step is represented by the attack of third OH radical equivalent on formerly formed HNO, which yields NO and water molecule. The reaction is completed in 0.20 ps. Key bond lengths for third and fourth reaction steps are depicted in **Figure *S*9** and for last step in **Figure *S*10**. The initial temperature of the system in this case was set to 250 K.

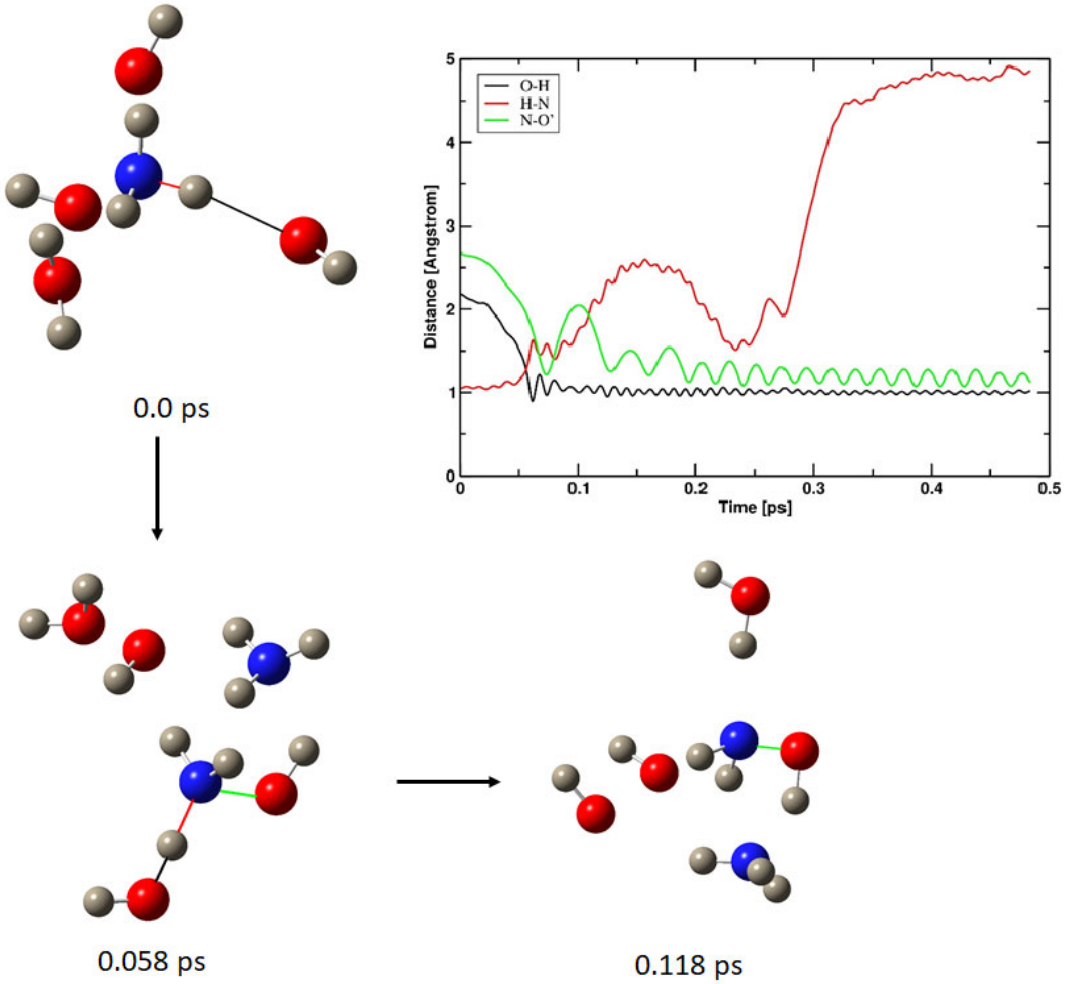


Figure S8. Sketch of the first and second reaction steps of ammonia with OH radicals. The most relevant bonding interactions deduced from Car-Parrinello simulations are highlighted.

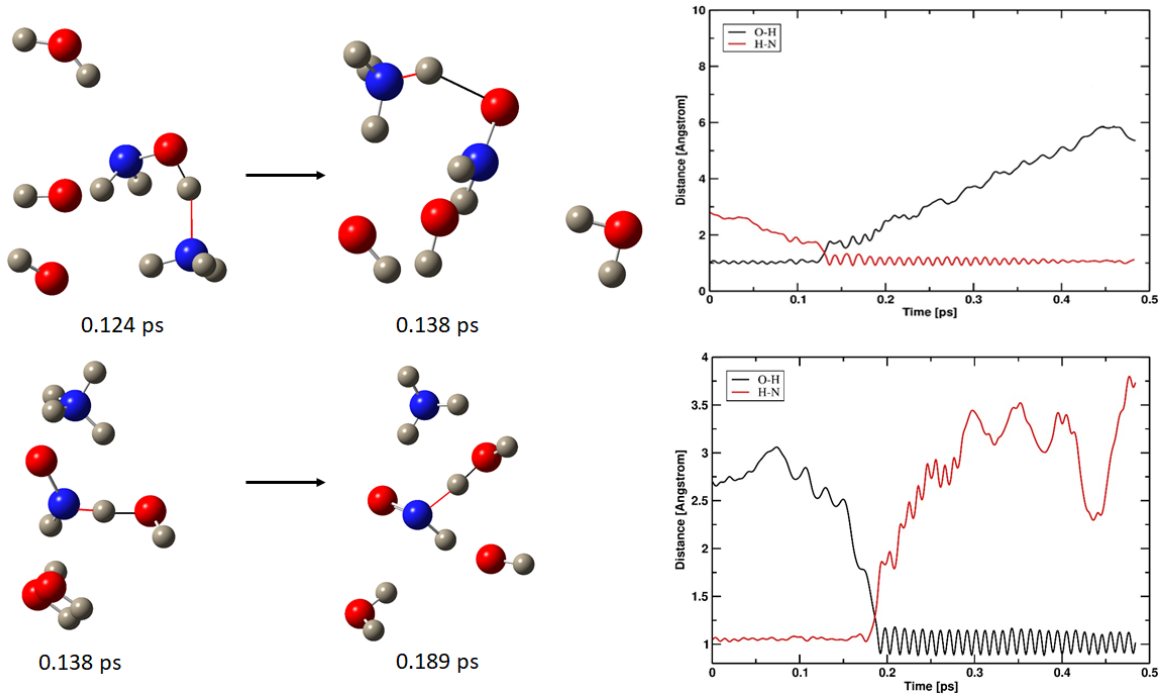


Figure S*9*. Sketch of the third and fourth reaction steps of ammonia with OH radical and NH_3 molecule. The most relevant bonding interactions deduced from Car-Parrinello simulations are highlighted.

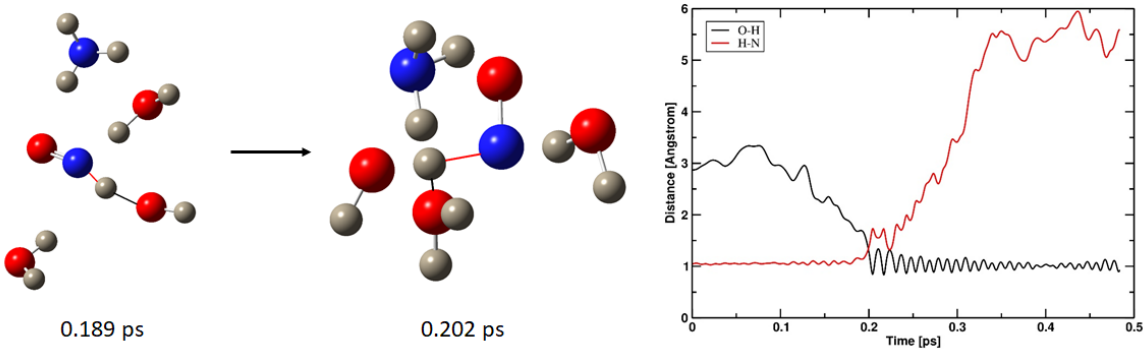


Figure S*10*. Sketch of the fifth reaction step of ammonia with OH radical. The most relevant bonding interactions deduced from Car-Parrinello simulations are highlighted.

<u>NH_2O formation mechanism in **System 1**:</u>

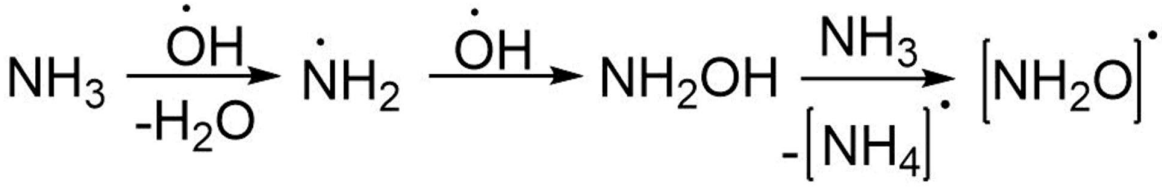


Figure S*11*. Sequence of elementary reaction steps that lead to the formation of NH_2O radical in **System 1**.

The first reaction step corresponds to the abstraction of hydrogen radical from ammonia by OH radical which results in the formation of NH_2 radical after 0.04 ps of simulation. The formed reactive intermediate is attacked further by second OH radical in 0.02 ps resulting in the formation of NH_2OH intermediate. Key bond lengths for first and second reaction steps are depicted in

Figure *S*12 . During the third step hydroxylamine reacts with second equivalent of NH_3 yielding NH_2O radical intermediate and neutral ammonium radical after 0.14 ps of simulation. Key bond lengths for last reaction step are depicted in **Figure *S*13**. The initial temperature of the system in this case was set to 300 K.

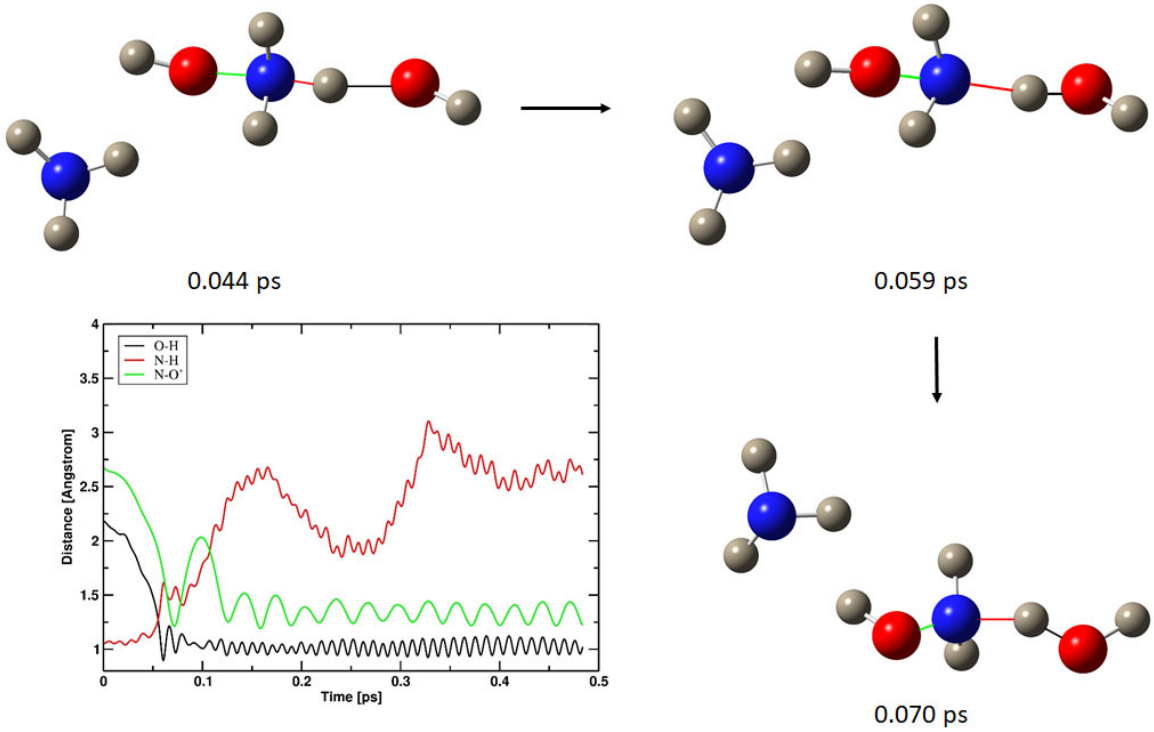


Figure S*12*. Sketch of the first and second reaction steps of ammonia with OH radicals. The most relevant bonding interactions deduced from Car-Parrinello simulations are highlighted.

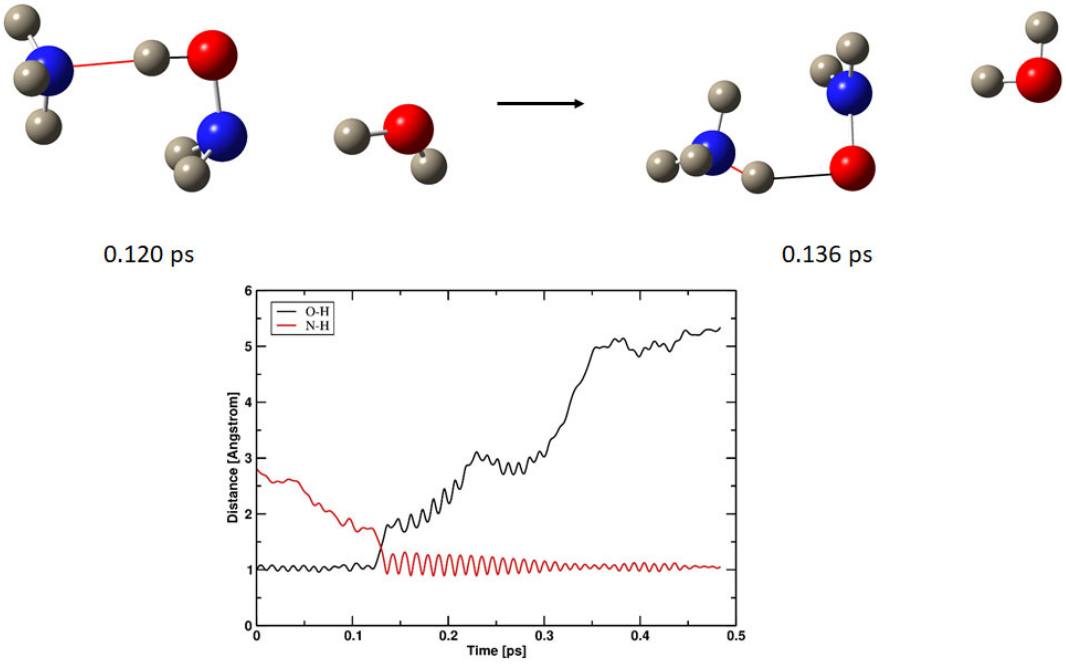


Figure S*13*. Sketch of the third reaction step of ammonia with OH radical. The most relevant bonding interactions deduced from Car-Parrinello simulations are highlighted.

NH_2OH formation mechanism 1 in **System 2**:

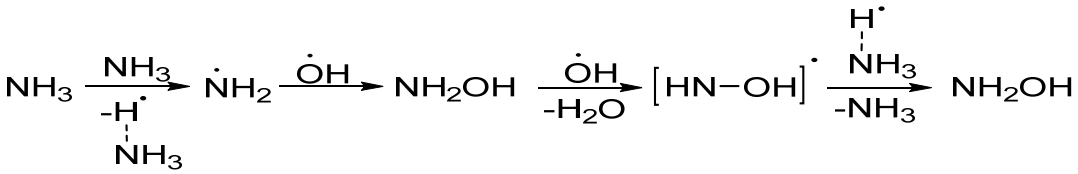


Figure S*14***.** Sequence of elementary reaction steps that lead to the formation of NH_2OH molecule in **system 2**.

The first reaction step corresponds to the homolytic dissociation of N-H bond, which results in the formation of NH_2 and H radicals after 0.15 ps of simulation. The formed hydrogen radical is coordinated by second equivalent of ammonia. Being more specific, hydrogen atom is located between two nitrogen centers. The second step is represented by the recombination of OH radical with NH_2 yielding closed shell hydroxylamine in 0.04 ps. The key bond lengths for the first and second reaction steps are depicted in **Figure *S***15. During the third step hydroxylamine reacts with second equivalent of OH radical yielding NHOH radical intermediate and water molecule in 0.01 ps. The last step is the recombination of NHOH radical with H radical and simultaneous loss of coordination by second equivalent of ammonia, which leads to the formation of stable closed-shell hydroxylamine. The reaction is completed in 0.23 ps. Key bond lengths for third and fourth reaction steps are depicted in **Figure *S***16. The initial temperature of the system in this case was set to 300 K.

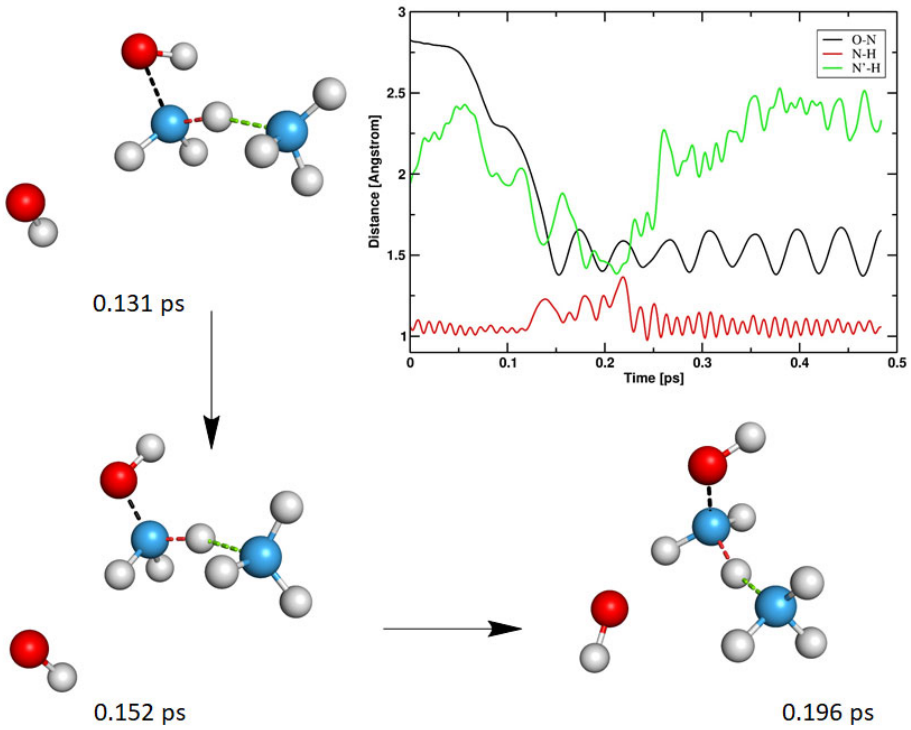


Figure S*15***.** Sketch of the first and second reaction steps of ammonia with OH radicals. The most relevant bonding interactions deduced from Car-Parrinello simulations are highlighted.

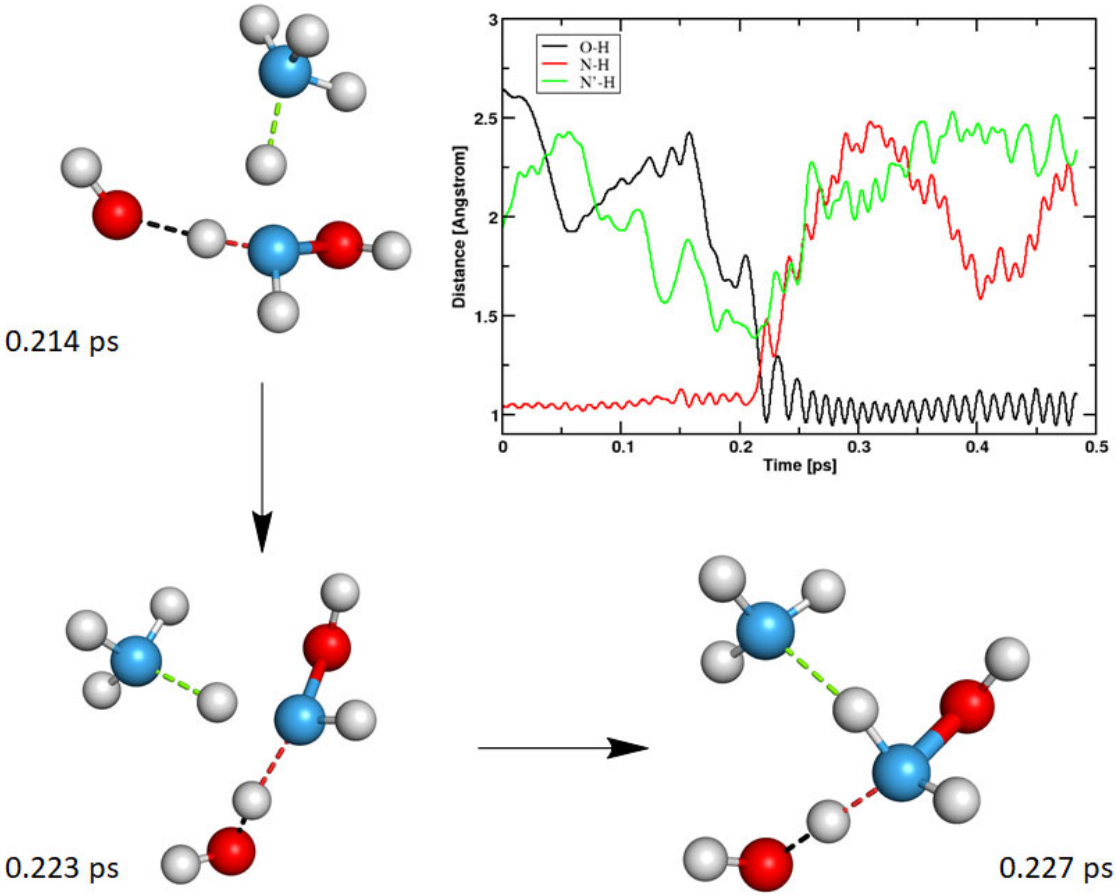


Figure S*16*. Sketch of the third and fourth reaction steps of ammonia with OH radical and NH_3 molecule. The most relevant bonding interactions deduced from Car-Parrinello simulations are highlighted.

<u>NH_2OH formation mechanism 2 in **System 2**:</u>

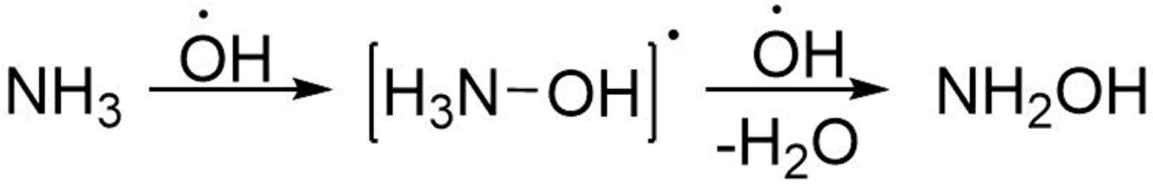


Figure S*17*. Second sequence of elementary reaction steps that lead to the formation of NH_2OH molecule in **system 2**.

The first reaction step corresponds to the attack of hydroxyl radical on ammonia, which results in the formation of NH_3OH radical after 0.07 ps of simulation. The formed reactive and very unstable intermediate is attacked further by second OH radical in less than 0.01 ps resulting in the formation of closed-shell NH_2OH product and water molecule. Key bond lengths for first and second reaction steps are depicted in **Figure *S*18**. The reaction is completed in 0.07 ps. The initial temperature of the system in this case was set to 300 K.

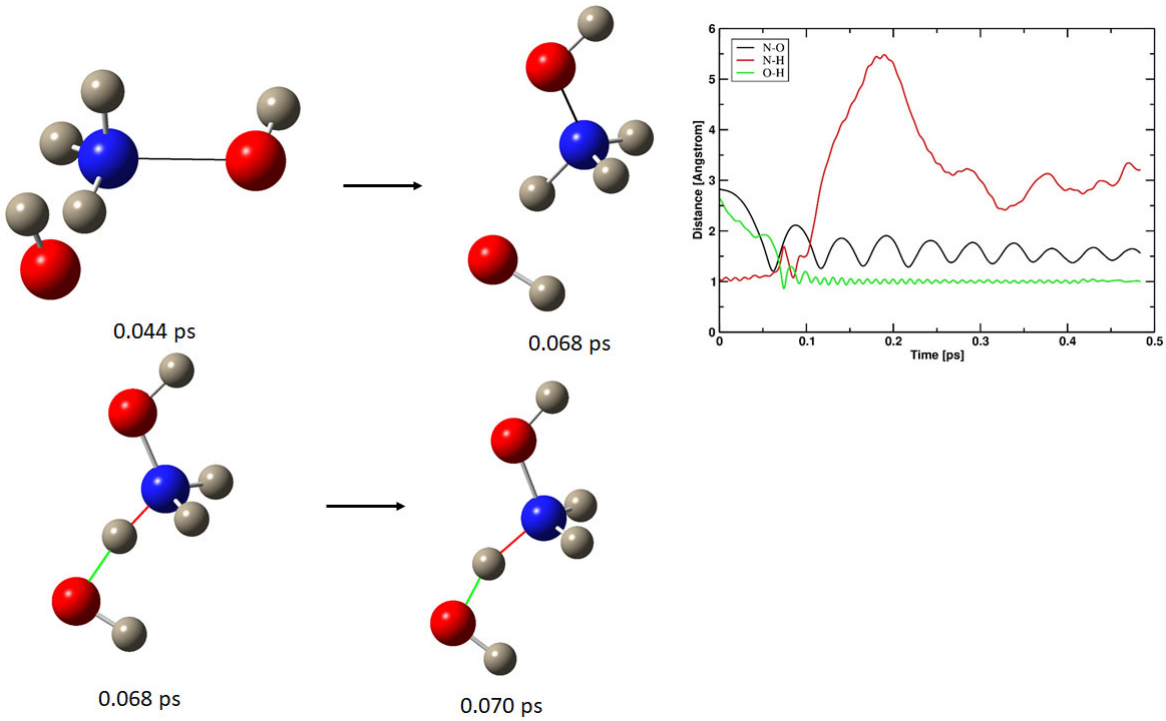


Figure S*18***.** Sketch of the first and second reaction steps of ammonia with OH radicals. The most relevant bonding interactions deduced from Car-Parrinello simulations are highlighted.

NHO formation mechanism 2 in **System 2**:

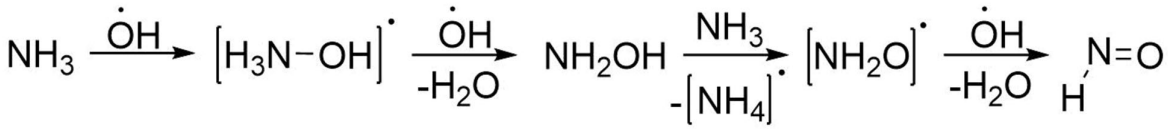


Figure S*19***.** Sequence of elementary reaction steps that lead to the formation of NHO molecule in **system 2**.

The first reaction step corresponds to the attack of hydroxyl radical on ammonia, which results in the formation of NH_3OH radical after 0.150 ps of simulation. The formed reactive and very unstable intermediate is attacked further by second OH radical in 0.005 ps resulting in the formation of closed-shell NH_2OH product and water molecule. Key bond lengths for first and second reaction steps are depicted in **Figure *S***20. During the third step hydroxylamine reacts with second equivalent of NH_3 yielding NH_2O radical intermediate and neutral ammonia radical after in 0.020 ps. The last step is the represented by attack of hydroxyl radical, which abstracts hydrogen radical yielding stable closed-shell NHO molecule and water. The reaction is completed in 0.394 ps. Key bond lengths for third and fourth reaction steps are depicted in **Figure *S***21. The initial temperature of the system in this case was set to 300 K.

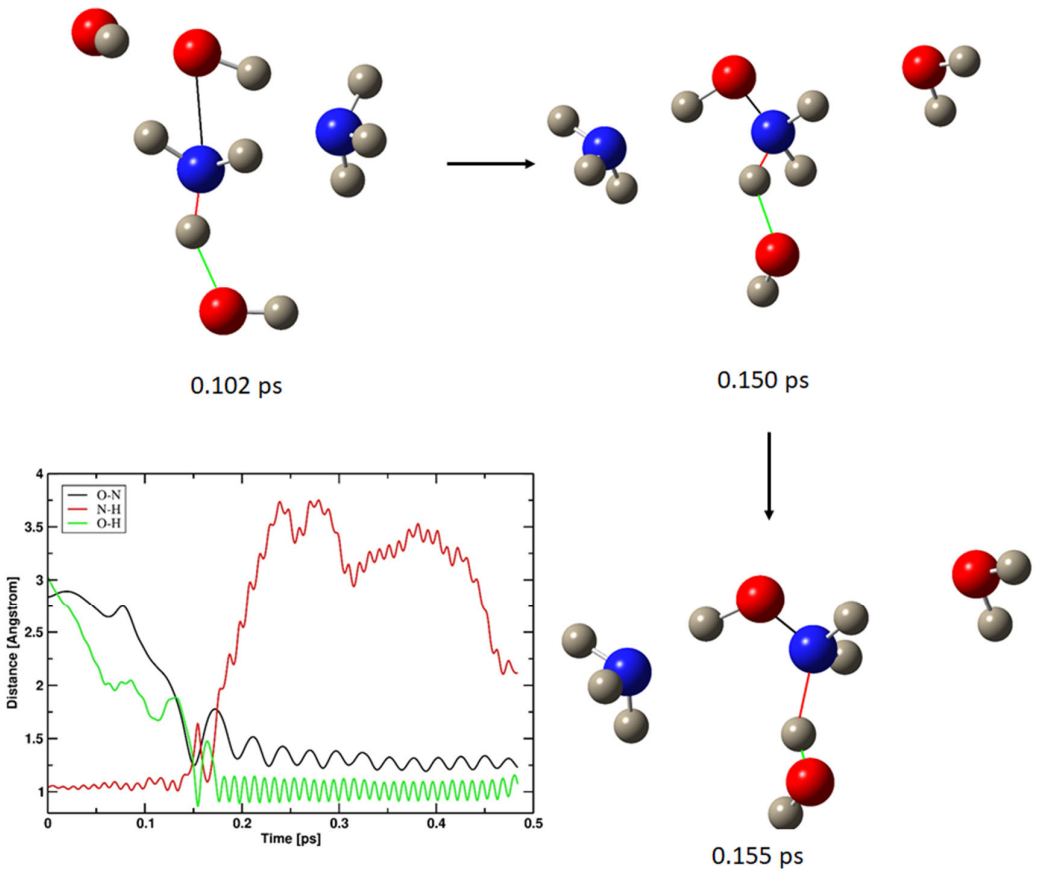


Figure S*20*. Sketch of the first and second reaction steps of ammonia with OH radicals. The most relevant bonding interactions deduced from Car-Parrinello simulations are highlighted.

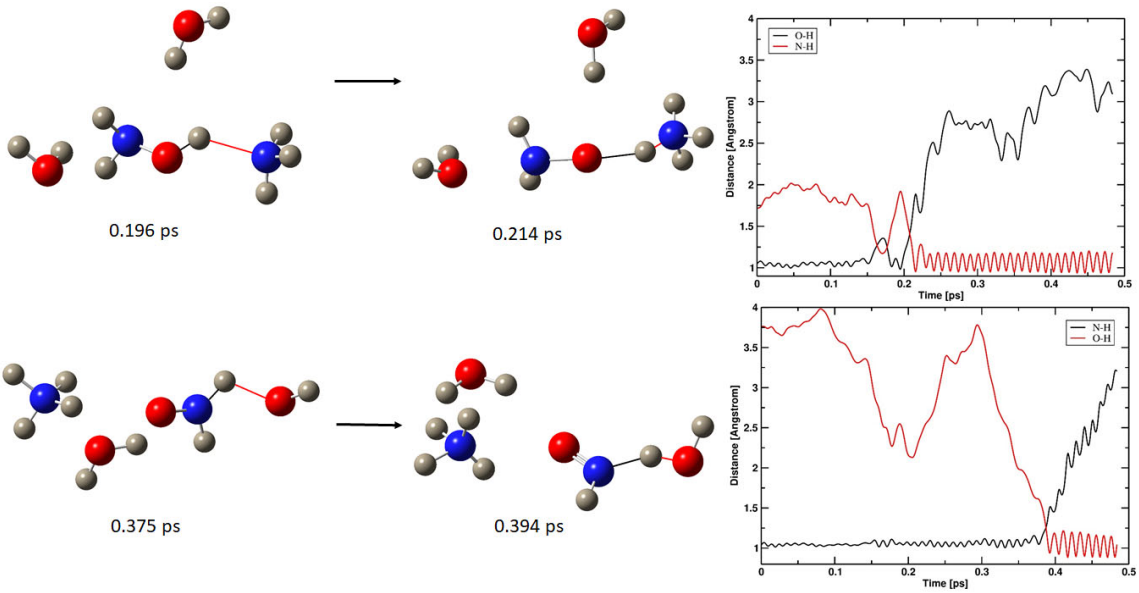


Figure S*21*. Sketch of the third and fourth reaction steps of ammonia with OH radical and NH_3 molecule. The most relevant bonding interactions deduced from Car-Parrinello simulations are highlighted.

In order to better simulate the real systems and the processes on cathodes, two new cells were created for each neutral equilibrated system, which differed only in the positions of created H radicals. As expected the formation of hydrogen molecules was observed. Furthermore, dissolved carbon dioxide was reduced to formic acid radical and the corresponding closed-shell acid.

HCOO radical formation mechanism in **Systems** 2 **and** 3:

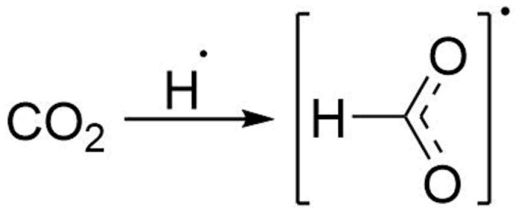


Figure S*22***.** Elementary reaction step that leads to the formation of HCOO radical in **System 1**.

The single reaction step corresponds to the attack of hydrogen radical on carbon in CO_2, which results in the formation of HCOO radical after 0.07 ps of simulation. Key bond length for first reaction step are depicted in **Figure *S***23. The same mechanism was observed in both 250 K and 300 K systems.

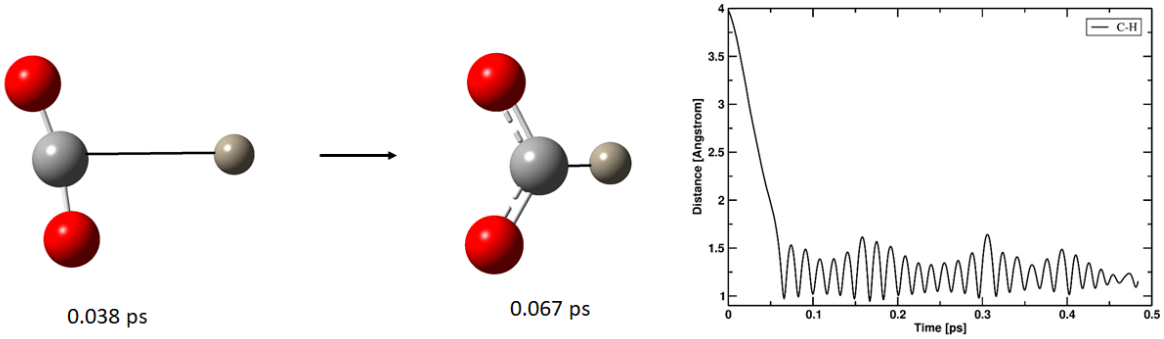


Figure S*23***.** Sketch of the single reaction step of hydrogen radical reaction with carbon dioxide. The relevant bonding interaction deduced from Car-Parrinello simulations is highlighted.

HCOOH formation mechanism in **system 2**:

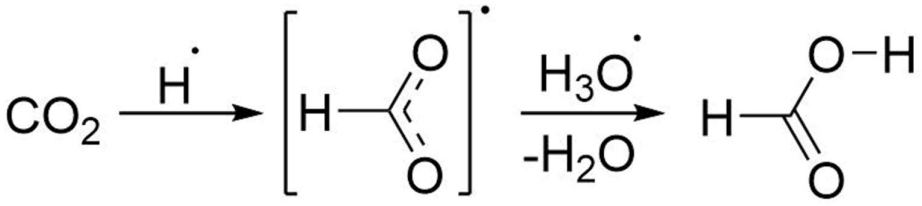


Figure S*24***.** Elementary reaction step that leads to the formation of HCOOH molecule in **system 2**.

The first reaction step corresponds to the attack of hydrogen radical on carbon in CO_2, which results in the formation of HCOO radical after 0.05 ps of simulation. The second reaction step is the hydrogen radical transfer from H_3O radical to formerly formed intermediate yielding closed-shell formic acid after 0.32 ps of simulation. Key bond length for first and second reaction steps are depicted in **Figure *S***25. The initial temperature of the system in this case was set to 300 K.

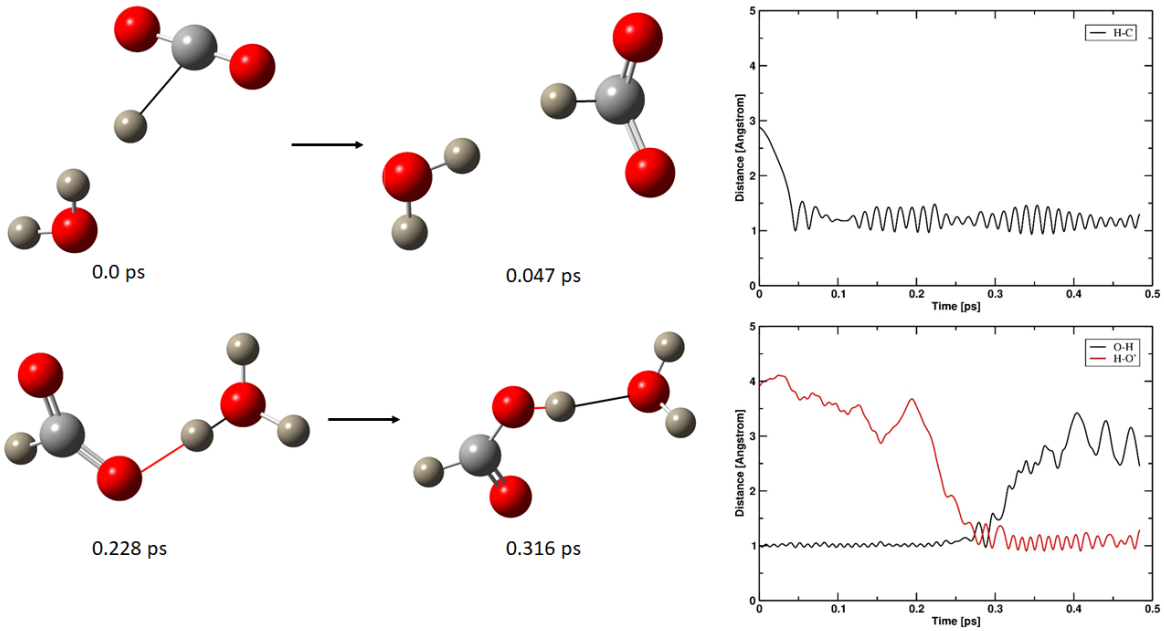


Figure S*25*. Sketch of the first and second reaction steps of hydrogen radical radical with carbon dioxide. The most relevant bonding interactions deduced from Car-Parrinello simulations is highlighted.

Method details for Ethanimine solutions

The simulation cells were 20 × 20 × 20 a.u.^{3} (10.6 ×10.6 ×10.6 Å^3). Solutions with a density of roughly 1.34 g/cm^3 were generated (4 ethanimine, 9 carbon dioxide and 21 water molecules named **system 3** or 4 ethanimine, 9 carbon dioxide and 22 water molecules named **System 4**). Density of the created solutions is higher than that of pure water (1.00 g/cm^3) because several water molecules are substituted with CO_2 and ethanimine, which have higher molecular weights. After equilibration of stable, neutral, closed-shell systems, reactive species were generated in two ways: by removing eight hydrogen radicals, leading to OH radicals in order to simulate anodic conditions and by removing eight OH radicals, leading to eight hydrogen radicals in order to simulate cathodic conditions.

Results and discussion

The most complex and important processes were observed during simulations of anodic conditions, that is why it makes more sense to begin the discussion with their detailed description. In order to better simulate the real systems, two new cells were created for each neutral equilibrated system, which differed only in the positions of created OH radicals. As expected the formation of various reactive oxygen based species was observed (e.g., hydrogen peroxide HOOH, HOO radical, O_2). Furthermore, ethanimine molecules were oxidized to several organic compounds, such as RNHO, nitrene radical, RNO radical, oxime. R is equal to CH_3CH=.

RNHO formation mechanism in **System 3**:

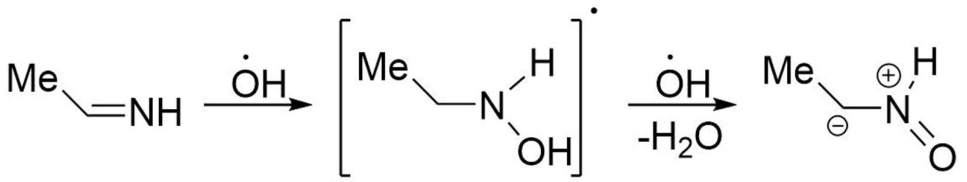


Figure S*26*. Sequence of elementary reaction steps that lead to the formation of RHNO molecule in **system 3**.

The first reaction step corresponds to the attack of hydroxyl radical on nitrogen atom of ethanimine, which results in the formation of RNHOH radical after 0.09 ps of simulation. The formed reactive intermediate is attacked further by second OH radical in 0.02 ps. As a result the stable closed-shell zwitter-ionic species is formed. Key bond lengths for first and second reaction steps are depicted in **Figure *S*27**. The process of zwitter-ion formation takes 0.27 ps according to Car-Parrinello MD simulation. The initial temperature of the system in this case was set to 250 K.

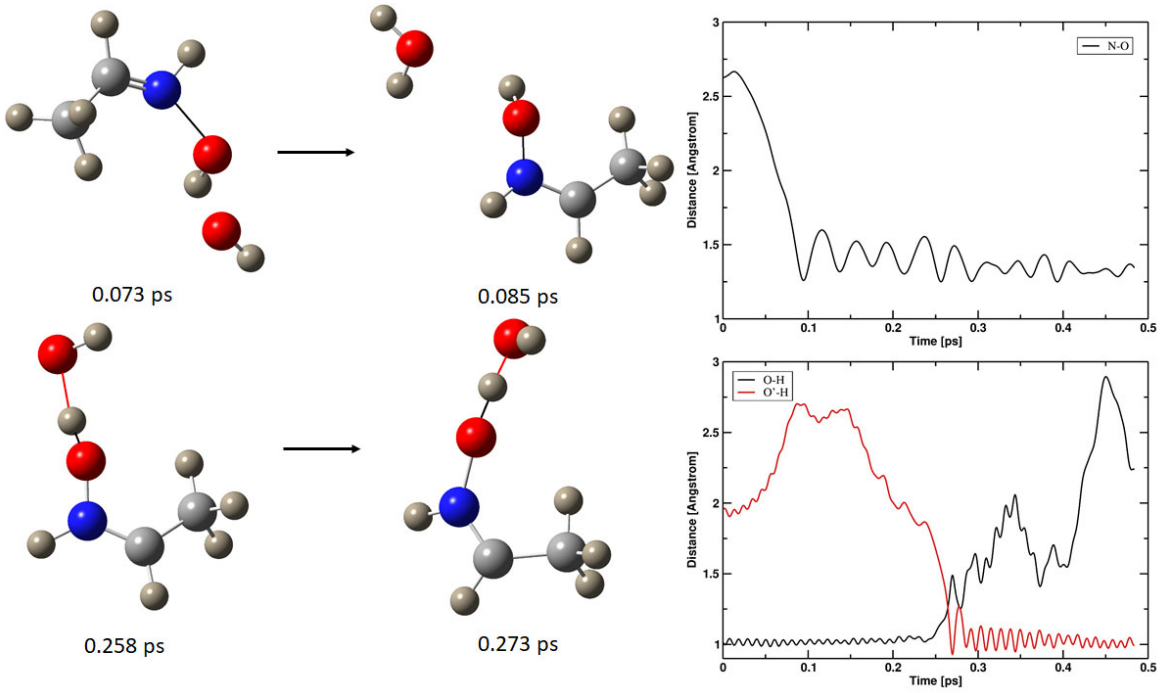


Figure S*27.* Sketch of the first and second reaction steps of ethanimine with OH radicals. The most relevant bonding interactions deduced from Car-Parrinello simulations are highlighted.

RNHO formation mechanism 2 in **System 3**:

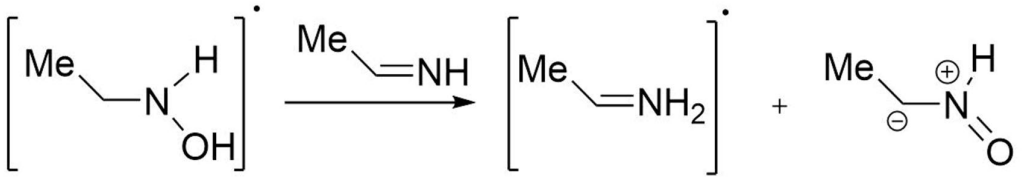


Figure S*28***.** Sequence of elementary reaction steps that lead to the formation of zwitter-ion in **system 3**.

The single reaction step corresponds to the hydrogen radical transfer between the unstable open-shell intermediate, which formation mechanism was clarified earlier in the report, and second equivalent of ethanimine. Reaction yields zwitter-ionic closed-shell species and ethylamine radical after 0.25 ps of simulation. Key bond lengths for single reaction step are depicted in **Figure *S***29. The initial temperature of the system in this case was set to 250 K.

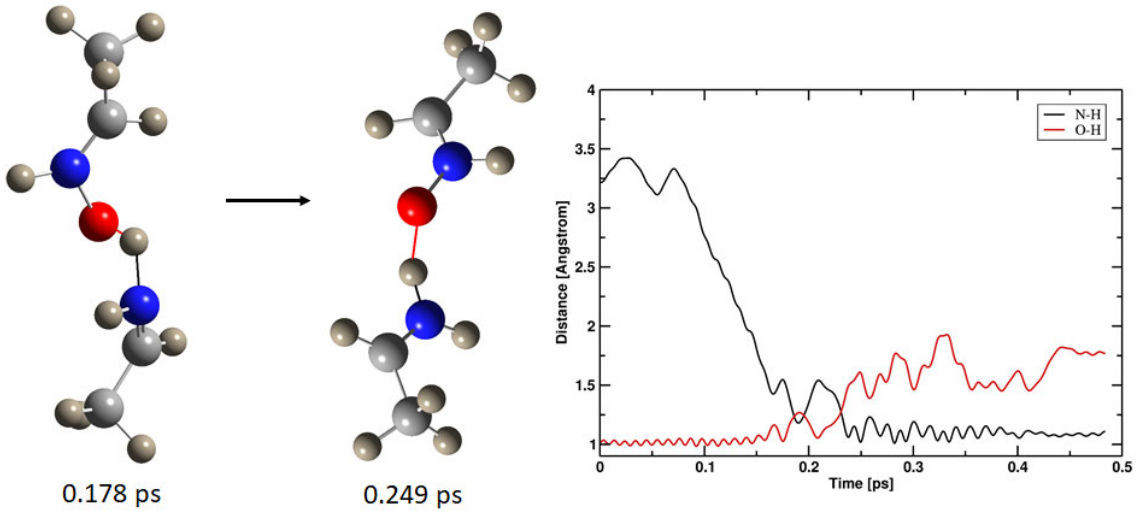
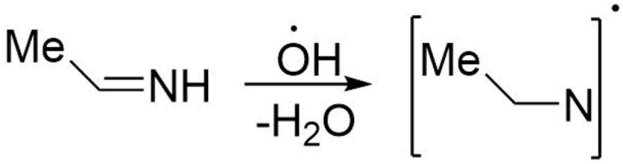


Figure S*29***.** Sketch of the single reaction step of RNHOH radical with second equivalent of ethanimine. The most relevant bonding interactions deduced from Car-Parrinello simulations are highlighted.

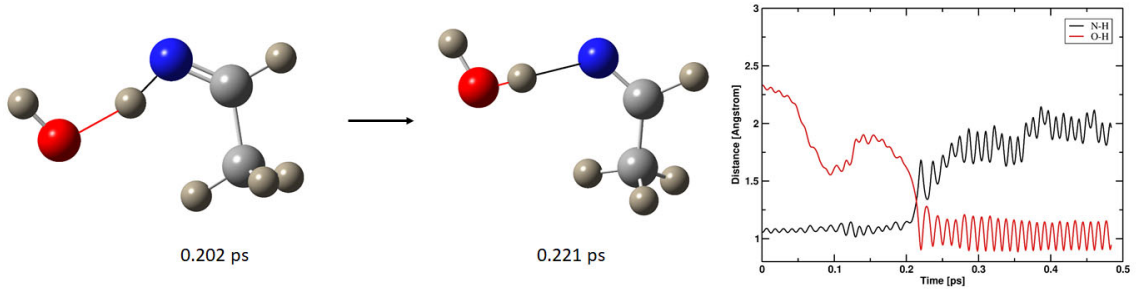
Nitrene radical formation mechanism in **System 3**:

Figure S*30***.** Sequence of elementary reaction step that leads to the formation of nitrene radical in **system 3**.



The single reaction step corresponds to the hydrogen radical abstraction by hydroxyl radical after 0.20 ps of simulation. The reaction is completed after 0.22 ps and yields nitrene radical. Key bond lengths for single reaction step are depicted in **Figure *S***31. The initial temperature of the system in this case was set to 250 K.

Figure S*31***.** Sketch of the single reaction step of ethanimine with hydroxyl radical. The most relevant bonding



interactions deduced from Car-Parrinello simulations are highlighted.

RNO radical formation mechanism 2 in **System 3**:

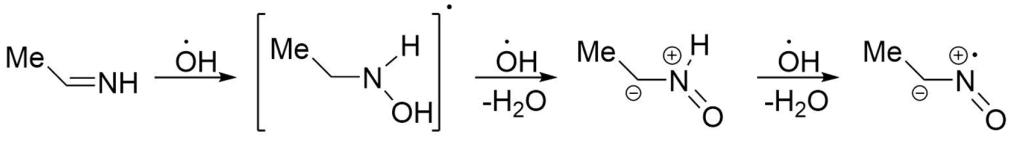


Figure S*32***.** Sequence of elementary reaction steps that lead to the formation of zwitter-ion radical in **system 3**.

The first reaction step corresponds to the attack of hydroxyl radical on nitrogen atom of ethanimine, which results in the formation of RNHOH radical after 0.08 ps of simulation. The formed reactive intermediate is attacked further by second OH radical in 0.03 ps. As a result the stable closed-shell zwitter-ionic species is formed. Key bond lengths for first and second reaction steps are depicted in **Figure *S*33**. The last step is represented by hydrogen radical abstraction by third equivalent of hydroxyl radical, which yields zwitter-ionic radical. The reaction is completed after 0.41 ps according to the Car-Parrinello MD simulation. Key bond lengths for third reaction step are depicted in **Figure *S*34**. The initial temperature of the system in this case was set to 300 K.

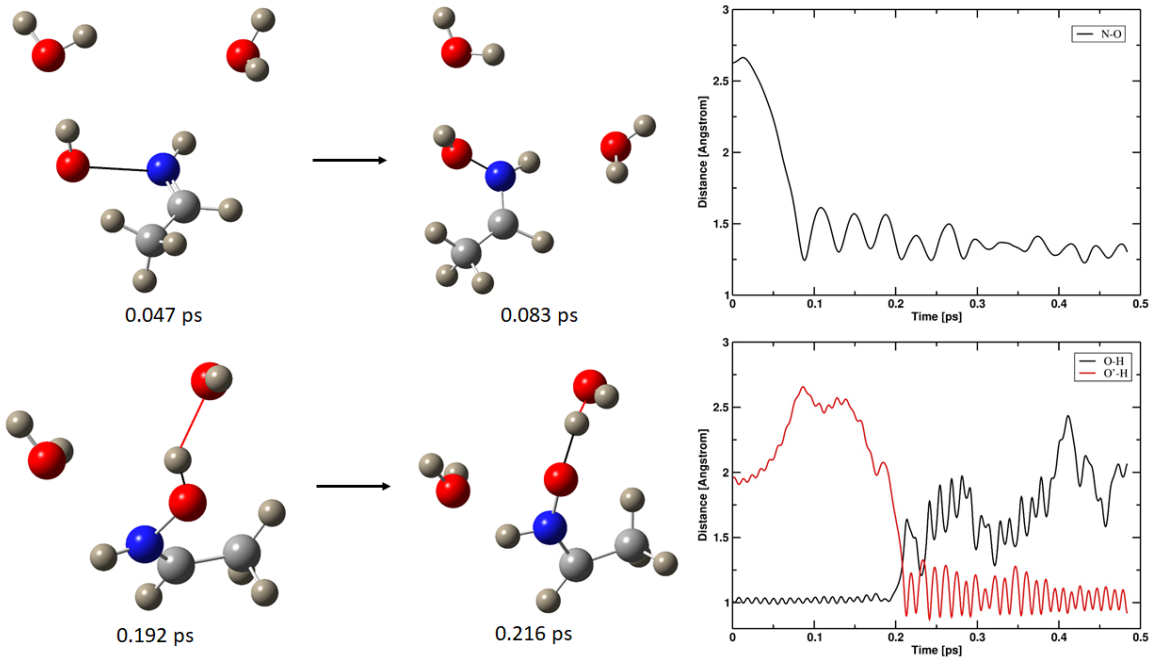


Figure S*33*. Sketch of the first and second reaction steps of ethanimine with OH radicals. The most relevant bonding interactions deduced from Car-Parrinello simulations are highlighted.

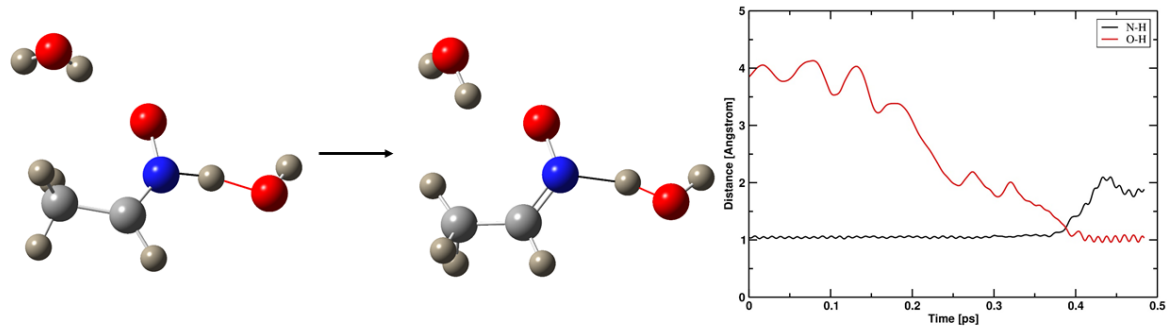


Figure S*34*. Sketch of the third reaction step of ethanimine with OH radicals. The most relevant bonding interactions deduced from Car-Parrinello simulations are highlighted.

Oxime formation mechanism in **System 4**:

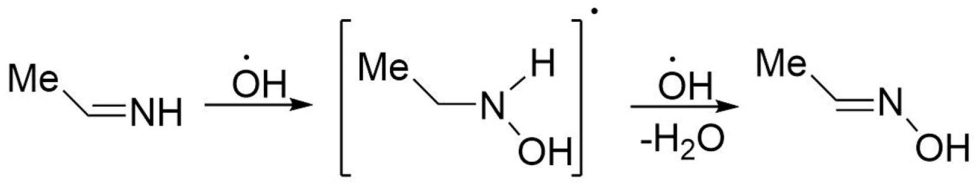


Figure S*35*. Sequence of elementary reaction steps that lead to the formation of oxime molecule in **System 4**.

The first reaction step corresponds to the attack of hydroxyl radical on nitrogen atom of ethanimine, which results in the formation of RNHOH radical after 0.08 ps of simulation. The formed reactive intermediate is attacked further by second OH radical in 0.01 ps, so reaction is completed in 0.11 ps. As a result two stable closed-shell species are formed: oxime and water molecule. Key bond lengths for first and second reaction steps are depicted in **Figure *S*36**. The initial temperature of the system in this case was set to 250 K.

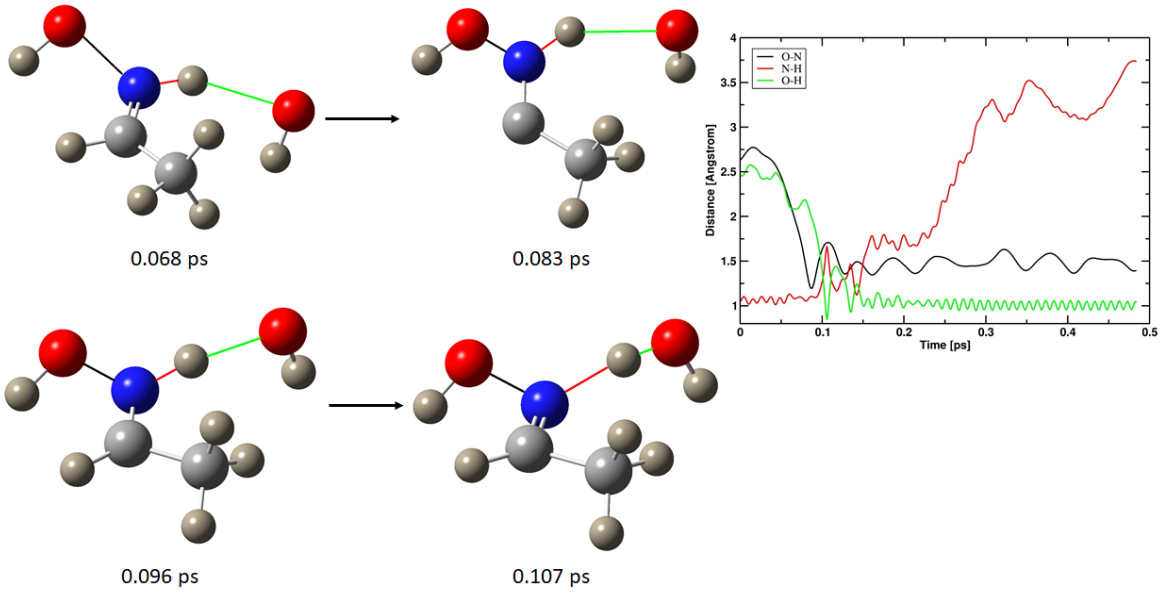


Figure S*36*. Sketch of the first and second reaction steps of ethanimine with OH radicals. The most relevant bonding interactions deduced from Car-Parrinello simulations are highlighted.

Oxime formation mechanism 2 in **System 4**:

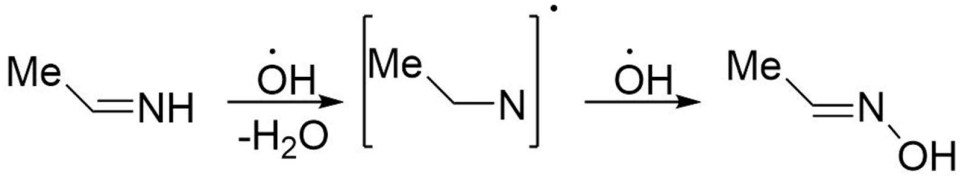


Figure S*37*. Sequence of elementary reaction steps that lead to the formation of oxime molecule in **System 4**.

The first reaction step corresponds to the hydrogen radical abstraction by hydroxyl radical after 0.05 ps of simulation. The first step is completed after 0.01 ps and yields nitrene radical. The second step is represented by the addition of second hydroxyl radical equivalent to previously

formed open-shell intermediate. The reaction is completed after 0.36 ps of simulation. . Key bond lengths for first and second reaction steps are depicted in **Figure S***38*. The initial temperature of the system in this case was set to 250 K.

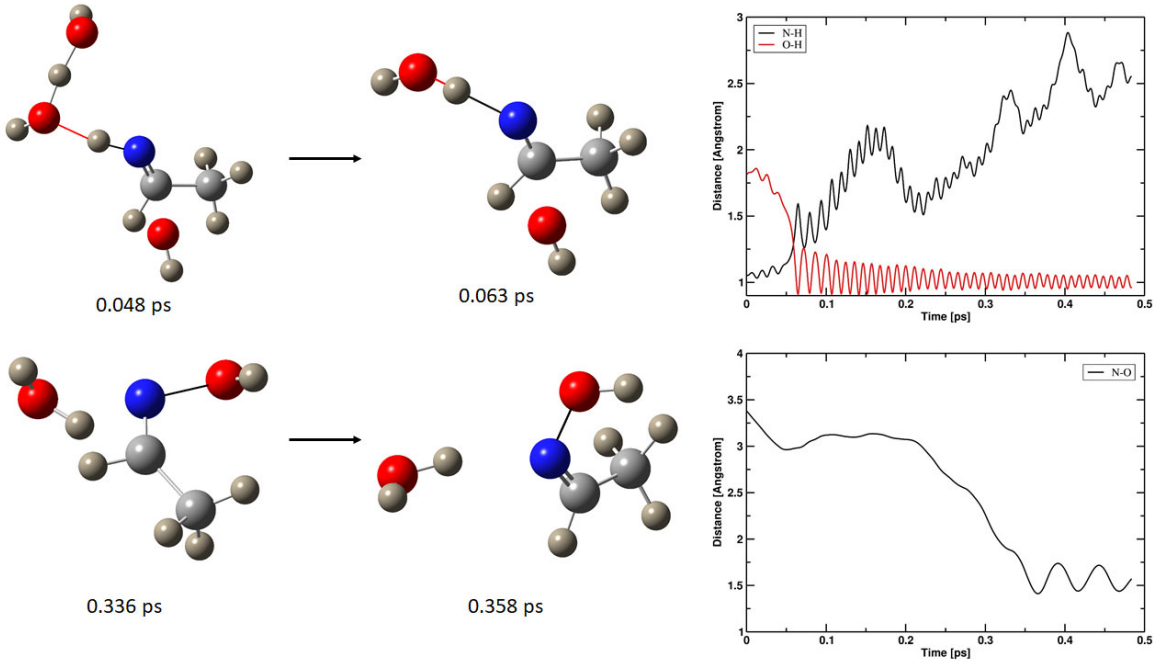


Figure S*38***.** Sketch of the first and second reaction steps of ethanimine with OH radicals. The most relevant bonding interactions deduced from Car-Parrinello simulations are highlighted.

In order to better simulate the real systems and the processes on cathodes, two new cells were created for each neutral equilibrated system, which differed only in the positions of created H radicals. As expected, the formation of hydrogen molecules was observed. Furthermore, dissolved carbon dioxide was reduced to formic acid radical. In addition, ethanimine was reduced to amine radical. Lastly, the addition reaction between carbon dioxide and ethanimine radical was observed, so new C-N σ-bond was formed.

Amine radical formation mechanism in **System 3**:

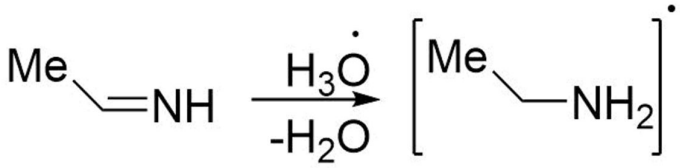


Figure S*39***.** Sequence of elementary reaction step that leads to the formation of amine radical in **system 3**.

The single reaction step corresponds to the hydrogen radical transfer to the nitrogen atom of ethanimine from hydroxonium radical. The reaction is completed after 0.03 ps and yields amine radical. Key bond lengths for single reaction step are depicted in **Figure S***40*. The initial temperature of the system in this case was set to 300 K.

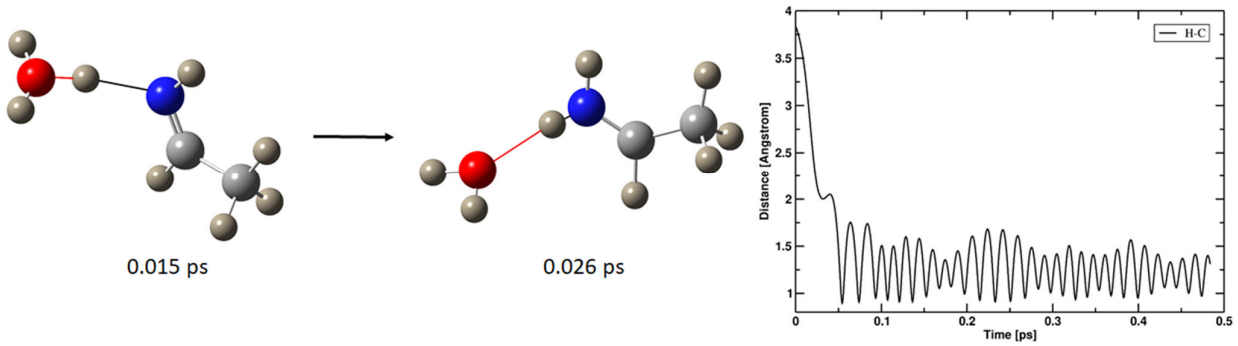


Figure S*40.* Sketch of the single reaction step of ethanimine with hydroxonium radical. The most relevant bonding interactions deduced from Car-Parrinello simulations are highlighted.

$CH_2CHNHCO_2$ radical formation mechanism in **System 4**:

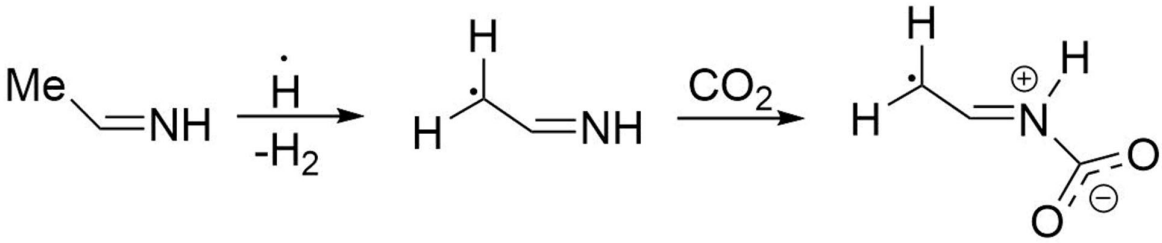


Figure S*41***.** Sequence of elementary reaction steps that lead to the formation of zwitter-ion radical in **System 4**.

The first reaction step corresponds to the hydrogen radical abstraction by free hydrogen radical after 0.04 ps of simulation. The first step is completed after 0.01 ps and yields imine radical. The second step is represented by the addition of previously formed reactive open-shell intermediate to carbon dioxide molecule, so new C-N σ-bond was formed. The reaction is completed after 0.36 ps of simulation. Key bond lengths for first and second reaction steps are depicted in **Figure *S***42. The initial temperature of the system in this case was set to 250 K.

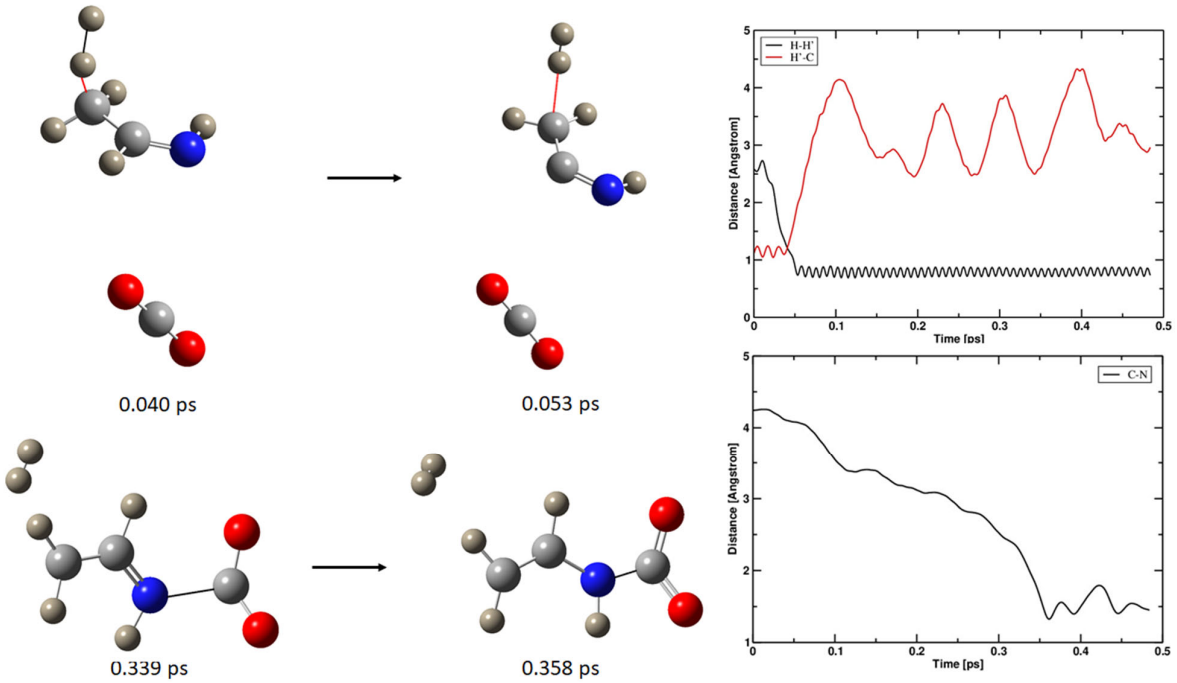


Figure S*42*. Sketch of the first and second reaction steps of ethanimine with hydrogen radical and carbon dioxide. The most relevant bonding interactions deduced from Car-Parrinello simulations are highlighted.

Amine radical formation mechanism in **System 4**:

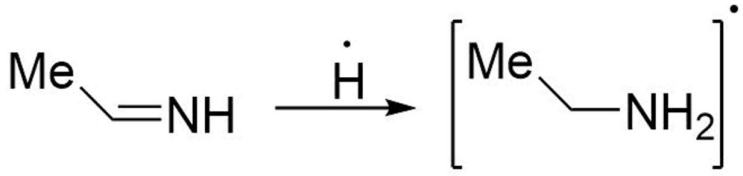


Figure S*43*. Sequence of elementary reaction step that leads to the formation of amine radical in **System 4**.

The single reaction step corresponds to the hydrogen radical addition to ethanimine after 0.01 ps of simulation. The first step is completed after 0.01 ps and yields amine radical. Key bond lengths for the single reaction steps are depicted in **Figure *S*44**. The initial temperature of the system in this case was set to 250 K.

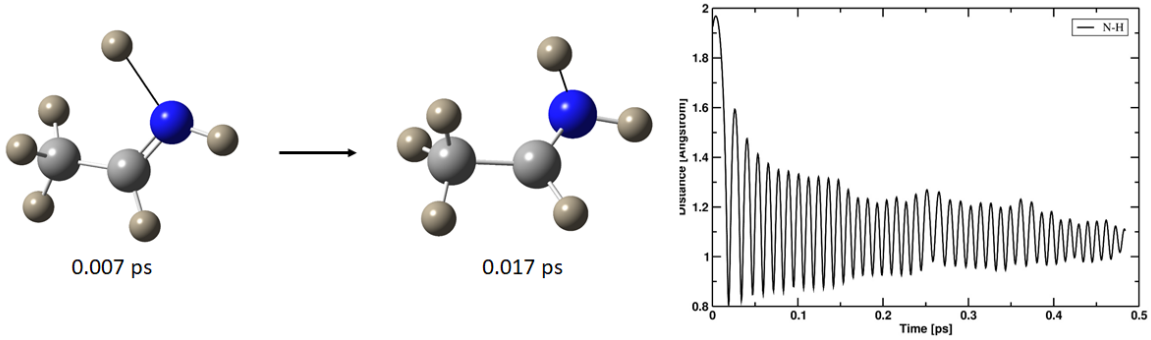


Figure S*44*. Sketch of the single reaction step of ethanimine with hydrogen radical. The most relevant bonding interactions deduced from Car-Parrinello simulations are highlighted

The mechanism of formation of HCOO radical is identical to that, which is described for ammonia solution/CO_2 solution – simple addition of hydrogen radical to carbon atom of CO_2.

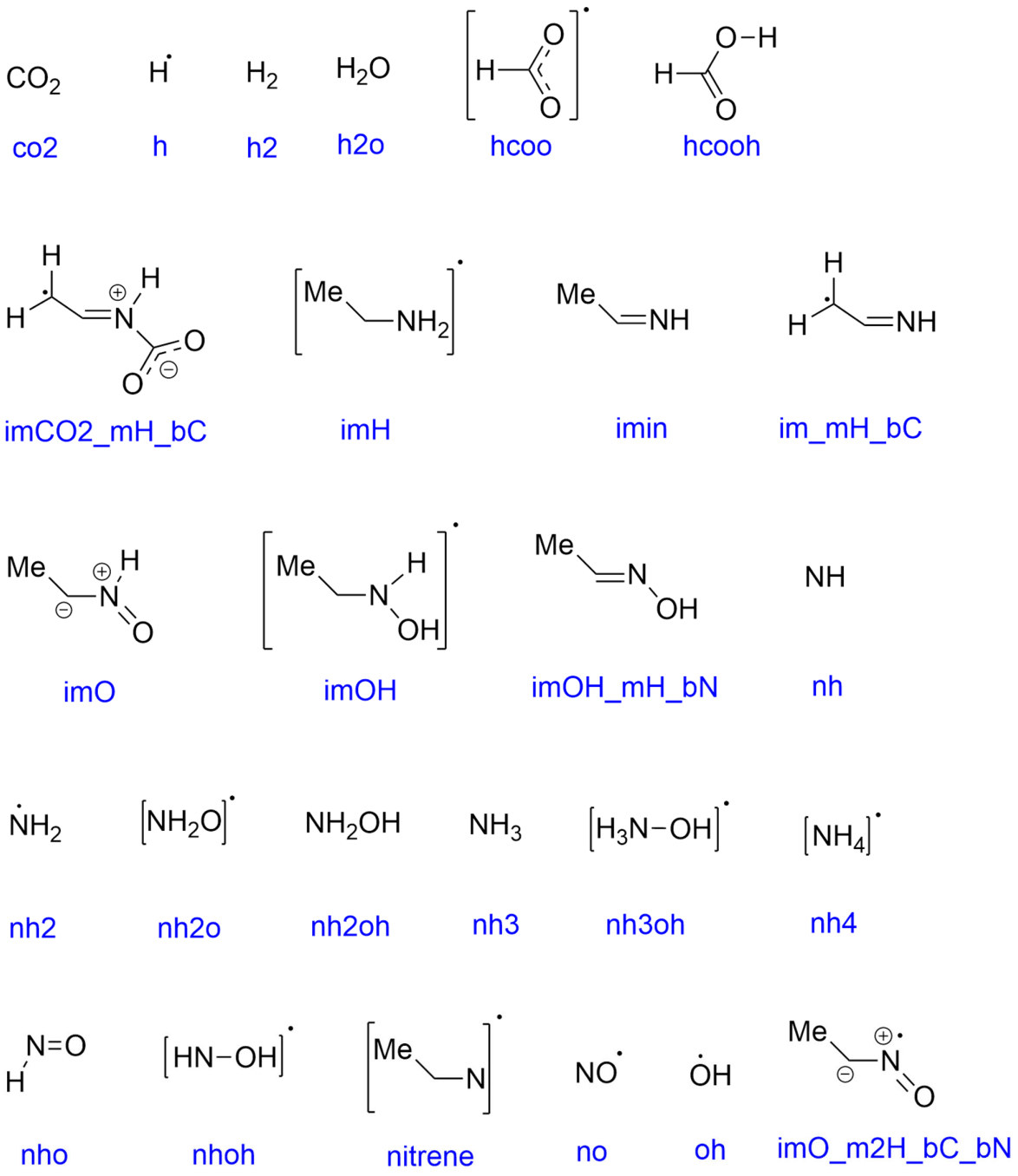


Figure S*45*. List of the used abbreviations for calculations and corresponding chemical structure.

Technical details of Gaussian calculations

All geometry optimizations and vibrational frequency calculations have been performed using the B3LYP-D3[9]/BLYP-D3**Error! Bookmark not defined.**,**Error! Bookmark not defined.**,**Error! Bookmark not defined.** hybrid functionals, B2PLYP-D3[10] double hybrid functional, second order Møller–Plesset perturbation method MP2[11], Hartree-Fock method and coupled cluster CCSD method in combination with the 6-311G(d,p) basis set[12]. Solvent effects for water have been taken into account with the PCM continuum solvation model[13]. Thermal corrections to enthalpies at

298.15 K have been calculated at the same level using the rigid rotor/harmonic oscillator model. The geometry optimizations have been performed with Gaussian 16 program package[14].

Table S1. Calculated thermodynamic properties for all reactants, intermediates and products, which were described above. The same basis set 6-311G(d,p) was used for all methods. All energies are given in Hartree/particle. The optimizations of structures marked with red color have not converged at all or converged to other species.

System_method	E_{tot} [Hartree]	H_{298} [Hartree]	G_{298} [Hartree]	Lowest frequency [cm^{-1}]
co2_b2plyp	-188.499065	-188.483955	-188.508237	654.892
co2_b3lyp	-188.643912	-188.628722	-188.652991	660.3284
co2_blyp	-188.6289466	-188.614224	-188.638566	625.8585
co2_ccsd	-188.1942803	-188.178948	-188.203193	676.6006
co2_hf	-187.6913505	-187.675177	-187.699297	753.3401
co2_mp2	-188.2012519	-188.186072	-188.210361	655.3421
h_b2plyp	-0.498633304	-0.496273	-0.509287	
h_b3lyp	-0.502177352	-0.499817	-0.512831	
h_blyp	-0.497577785	-0.495217	-0.508232	
h_ccsd	-0.499826467			
h_hf	-0.499826467	-0.497466	-0.510481	
h_mp2	-0.499826467	-0.497466	-0.510481	
h2_b2plyp	-1.168496794	-1.155027	-1.169816	4462.1437
h2_b3lyp	-1.179723836	-1.166367	-1.181163	4412.4222
h2_blyp	-1.169315814	-1.156127	-1.170933	4338.5826
h2_ccsd	-1.168484791	-1.155124	-1.169918	4414.5681
h2_hf	-1.13266269	-1.118908	-1.133683	4586.9018
h2_mp2	-1.160428384	-1.146811	-1.161593	4526.6479
h2o_b2plyp	-76.3893697	-76.364067	-76.385491	1658.8541
h2o_b3lyp	-76.45465114	-76.429603	-76.451034	1642.0633
h2o_blyp	-76.43537586	-76.411036	-76.432499	1614.9575
h2o_ccsd	-76.27861526	-76.25301	-76.274429	1694.3492
h2o_hf	-76.05472421	-76.027991	-76.049355	1751.3266
h2o_mp2	-76.2712825	-76.245714	-76.267137	1673.7915
h2o2_b2plyp_g	-151.46808	-151.437205	-151.46373	350.6753
h2o2_b3lyp_g	-151.5922112	-151.561556	-151.588091	347.2612
h2o2_b3lyp_g_nb	-151.632249	-151.601602	-151.628065	377.7154
h2o2_blyp_g	-151.5744174	-151.545017	-151.57171	321.0237
h2o2_ccsd_g	-151.2421295	-151.210796	-151.237244	375.8619
h2o2_hf_g	-150.8203843	-150.786698	-150.812981	394.417
h2o2_mp2_g	-151.2313966	-151.200258	-151.226738	366.9056
h3o_b2plyp	-76.84350397	-76.826637	-76.848668	-1029.5394
h3o_b3lyp	-76.91963071	-76.902942	-76.924992	-1030.0631
h3o_blyp	-76.90594231	-76.88723	-76.911683	-1098.2967
h3o_ccsd	-76.72296693	-76.694543	-76.717659	-738.8374
h3o_hf	-76.47622279	-76.459513	-76.481466	-4079.9231
h3o_mp2	-76.71523322	-76.680373	-76.703476	-731.8697
hcoo_b2plyp	-188.9856854	-188.874057	-188.901842	656.614
hcoo_b3lyp	-189.1412359	-189.117583	-189.145433	658.0949
hcoo_blyp	-189.1255694	-189.102082	-189.129975	631.4709
hcoo_ccsd	-188.6760219	-188.651268	-188.679082	658.7706
hcoo_hf	-188.1529124	-188.125881	-188.153589	707.8331
hcoo_mp2	-188.6673856	-188.640672	-188.668456	676.628
hcooh_b2plyp	-189.6647921	-189.626822	-189.655054	549.5341
hcooh_b3lyp	-189.8235769	-189.785918	-189.814153	548.676
hcooh_blyp	-189.7917104	-189.755334	-189.783645	548.3113
hcooh_ccsd	-189.362621	-189.324091	-189.352325	530.4997
hcooh_hf	-188.8255074	-188.78487	-188.81299	541.0675
hcooh_mp2	-189.3538537	-189.315577	-189.343813	544.0549
imCO2_mH_bC_b2plyp	-321.6878313	-321.610272	-321.649134	40.3735
imCO2_mH_bC_b3lyp_neu	-321.9780999	-321.906331	-321.950774	3.789
imCO2_mH_bC_blyp_neu	-321.9090095	-321.839004	-321.88267	12.7975

imCO2_mH_bC_ccsd	-321.1393132	-321.061099	-321.09935	39.7284
imCO2_mH_bC_hf	-320.1715713	-320.089289	-320.126487	56.1762
imCO2_mH_bC_mp2	-321.1077683	-321.028844	-321.066656	56.1818
imH_b2plyp	-134.4140098	-134.329368	-134.360859	190.4444
imH_b3lyp	-134.5690013	-134.485271	-134.516823	189.002
imH_blyp	-134.4971482	-134.415563	-134.447213	187.7648
imH_ccsd	-134.1761423	-134.091015	-134.12248	191.7956
imH_hf	-133.6727542	-133.583994	-133.615331	199.9545
imH_mp2	-134.1368102	-134.051329	-134.082714	197.7723
imin_b2plyp	-133.8542854	-133.780543	-133.810254	200.1185
imin_b3lyp	-134.0015393	-133.928423	-133.958138	200.3282
imin_blyp	-133.9386302	-133.867492	-133.897293	198.5075
imin_ccsd	-133.6171582	-133.543004	-133.572763	190.3409
imin_hf	-133.1175383	-133.039749	-133.069317	200.6859
imin_mp2	-133.5852945	-133.511132	-133.540864	197.0129
im_mH_bC_b2plyp	-133.2003208	-133.140296	-133.169777	492.7794
im_mH_bC_b3lyp	-133.3462805	-133.286732	-133.31621	497.2189
im_mH_bC_blyp	-133.3462805	-133.286732	-133.31621	497.2189
im_mH_bC_ccsd	-132.9645157	-132.90456	-132.934092	489.7155
im_mH_bC_hf	-132.5070601	-132.444724	-132.474097	516.2048
im_mH_bC_mp2	-132.9207383	-132.860111	-132.889561	497.9723
imO_b2plyp	-208.9869287	-208.907495	-208.939771	172.4528
imO_b3lyp	-209.1934594	-209.114601	-209.146877	173.7369
imO_blyp	-209.1321509	-209.055625	-209.088132	163.5182
imO_ccsd	-208.6266389	-208.546637	-208.578941	164.3117
imO_hf	-207.927522	-207.84329	-207.87522	189.7924
imO_mp2	-208.5981804	-208.518393	-208.550717	163.5335
imOH_b2plyp	-209.5445979	-209.454712	-209.489627	120.6223
imOH_b3lyp	-209.7569497	-209.668104	-209.703241	103.852
imOH_blyp	-209.700998	-209.616184	-209.655524	26.7429
imOH_ccsd	-209.1930174	-209.102308	-209.137124	125.634
imOH_hf	-208.4951083	-208.399925	-208.434425	129.843
imOH_mp2	-209.1521522	-209.061294	-209.096053	130.7674
imOH_mH_bN_b2plyp	-209.0014635	-208.922711	-208.955336	207.2957
imOH_mH_bN_b3lyp	-209.2058645	-209.127699	-209.160312	206.449
imOH_mH_bN_blyp	-209.1415737	-209.0657	-209.098512	202.8723
imOH_mH_bN_ccsd	-208.649237	-208.56985	-208.602532	197.7613
imOH_mH_bN_hf	-207.9516962	-207.868178	-207.900543	211.87
imOH_mH_bN_mp2	-208.6175249	-208.538314	-208.570966	204.5363
nh_b2plyp	-55.1074703	-55.096468	-55.115973	3378.8893
nh_b3lyp	-55.15986626	-55.149011	-55.168524	3314.3905
nh_blyp	-55.14387582	-55.133319	-55.152853	3183.1602
nh_ccsd	-55.03162485	-55.020615	-55.040122	3382.3383
nh_hf	-54.87417249	-54.862632	-54.882105	3614.9212
nh_mp2	-55.00300275	-54.991831	-55.01133	3453.0536
nh2_b2plyp	-55.84291973	-55.819904	-55.841999	1548.6131
nh2_b3lyp	-55.90042243	-55.877679	-55.899783	1537.3321
nh2_blyp	-55.87820826	-55.856105	-55.87824	1509.4878
nh2_ccsd	-55.75608863	-55.733048	-55.755148	1555.9677
nh2_hf	-55.58470778	-55.560553	-55.582599	1645.6592
nh2_mp2	-55.73809272	-55.714755	-55.736844	1550.2646
nh2o_b2plyp	-131.0220263	-130.991034	-131.01805	268.5947
nh2o_b3lyp	-131.1388482	-131.108219	-131.135343	237.0175
nh2o_blyp	-131.1154611	-131.085837	-131.112783	309.5937
nh2o_ccsd	-130.8139776	-130.782523	-130.809226	402.3499
nh2o_hf	-130.4406197	-130.407437	-130.433945	512.5231
nh2o_mp2	-130.7972656	-130.765657	-130.792635	272.8872
nh2oh_b2plyp	-131.6445913	-131.599836	-131.626587	347.4558
nh2oh_b3lyp	-131.7637625	-131.719442	-131.746213	344.7759
nh2oh_blyp	-131.7328876	-131.690131	-131.717046	320.3481

nh2oh_ccsd	-131.440621	-131.39539	-131.422099	355.6583
nh2oh_hf	-131.0345713	-130.986617	-131.013204	370.8117
nh2oh_mp2	-131.4243198	-131.379156	-131.405873	354.9606
nh3_b2plyp	-56.51950706	-56.481111	-56.502943	1146.8437
nh3_b3lyp	-56.58150412	-56.543458	-56.565298	1122.6655
nh3_blyp	-56.5534748	-56.516393	-56.538259	1115.658
nh3_ccsd	-56.42865509	-56.390104	-56.412973	1186.0567
nh3_hf	-56.21601373	-56.175719	-56.197509	1197.3373
nh3_mp2	-56.41433369	-56.375658	-56.398526	1170.3882
nh3oh_b2plyp				
nh3oh_b3lyp	-132.2697245	-132.222005	-132.252218	180.4939
nh3oh_blyp	-132.2362443	-132.190062	-132.220924	106.4821
nh3oh_ccsd	-131.9097511			
nh3oh_hf	-131.5089493			
nh3oh_mp2	-131.9243912			
nh4_b2plyp	-57.00115128	-56.959749	-56.981648	1189.5632
nh4_b3lyp	-57.07141073	-57.031271	-57.053191	1153.8173
nh4_blyp	-57.04340922	-57.00495	-57.026933	1076.2978
nh4_ccsd	-56.90479196	-56.859645	-56.88153	1223.1541
nh4_hf	-56.66976181	-56.628611	-56.650416	1344.1285
nh4_mp2	-56.88941259	-56.841318	-56.863211	1200.5974
nho_b2plyp	-130.4070513	-130.389126	-130.414178	1569.9426
nho_b3lyp	-130.5131278	-130.495262	-130.520306	1575.2019
nho_blyp	-130.5003897	-130.483423	-130.508512	1508.9944
nho_ccsd	-130.2057828	-130.187536	-130.212581	1598.5084
nho_hf	-129.8292959	-129.80942	-129.834376	1718.4638
nho_mp2	-130.1973593	-130.179349	-130.204418	1524.7493
nhoh_b2plyp	-131.0064842	-130.97524	-131.001719	762.3481
nhoh_b3lyp	-131.1216311	-131.090703	-131.117195	750.2137
nhoh_blyp	-131.09901	-131.069164	-131.095726	740.0333
nhoh_ccsd	-130.8030234	-130.771531	-130.798011	741.2826
nhoh_hf	-130.4307378	-130.397582	-130.424013	708.7977
nhoh_mp2	-130.7839754	-130.752301	-130.778757	773.1111
nitren_b2plyp	-133.2061238	-133.146197	-133.176496	191.4794
nitren_b3lyp	-133.3502191	-133.290902	-133.321209	190.9667
nitren_blyp	-133.2942087	-133.236496	-133.266915	186.2428
nitren_ccsd	-132.9721076	-132.911915	-132.942252	183.1379
nitren_hf	-132.5133667	-132.450885	-132.481076	187.3685
nitren_mp2	-132.8977367	-132.831088	-132.861864	151.1252
no_b2plyp	-129.8285743	-129.820897	-129.844201	1919.2017
no_b3lyp	-129.9273377	-129.919504	-129.942797	1987.8055
no_blyp	-129.9200297	-129.912493	-129.935815	1857.037
no_ccsd	-129.6267536	-129.619053	-129.642351	1930.2001
no_hf	-129.2837571	-129.275382	-129.298624	2225.3919
no_mp2	-129.6199095	-129.608721	-129.631991	3460.7472
oh_b2plyp	-75.69822262	-75.686336	-75.70656	3767.1405
oh_b3lyp	-75.75930628	-75.747566	-75.767799	3702.7338
oh_blyp	-75.74449341	-75.733086	-75.75334	3556.5912
oh_ccsd	-75.59105008	-75.579095	-75.599316	3797.6343
oh_hf	-75.4159556	-75.403445	-75.423633	4040.8352
oh_mp2	-75.57774331	-75.565671	-75.585887	3848.7693
imO_m2H_bC_bN_b2plyp	-208.3630764	-208.296885	-208.329615	178.1676
imO_m2H_bC_bN_b3lyp	-208.5678018	-208.502038	-208.535591	73.7237
imO_m2H_bC_bN_blyp	-208.514517	-208.450539	-208.484335	66.1859
imO_m2H_bC_bN_ccsd	-208.0052477	-207.938808	-207.971528	175.417
imO_m2H_bC_bN_hf	-207.3384443	-207.270478	-207.303121	185.4825
imO_m2H_bC_bN_mp2	-207.9220019	-207.85737	-207.891382	107.7611

Table S*2*. Cartesian coordinates of optimized structure of **nh3.** Calculations were performed at the PCM(H_2O)/BLYP-D3/6-311G(d,p) level of theory.

	x	y	z
N	0.00000000	0.00000000	0.12428600
H	0.00000000	0.93876600	-0.29000100
H	-0.81299500	-0.46938300	-0.29000100
H	0.81299500	-0.46938300	-0.29000100

Table S*3*. Cartesian coordinates of optimized structure of **oh.** Calculations were performed at the PCM(H_2O)/BLYP-D3/6-311G(d,p) level of theory.

	x	y	z
O	0.00000000	0.00000000	0.10963000
H	0.00000000	0.00000000	-0.87704200

Table S*4*. Cartesian coordinates of optimized structure of **h2o.** Calculations were performed at the PCM(H_2O)/BLYP-D3/6-311G(d,p) level of theory.

	x	y	z
O	0.00000000	0.00000000	0.12170600
H	0.00000000	0.75932000	-0.48682300
H	0.00000000	-0.75932000	-0.48682300

Table S*5*. Cartesian coordinates of optimized structure of **nh2.** Calculations were performed at the PCM(H_2O)/BLYP-D3/6-311G(d,p) level of theory.

	x	y	z
N	0.00000000	0.00000000	0.14638800
H	0.00000000	0.80431300	-0.51235800
H	0.00000000	-0.80431300	-0.51235800

Table S*6*. Cartesian coordinates of optimized structure of **nh2oh.** Calculations were performed at the PCM(H_2O)/BLYP-D3/6-311G(d,p) level of theory.

	x	y	z
N	0.71034700	0.00008900	0.15922400
H	1.05325600	-0.81216200	-0.37110800
H	1.05358500	0.81160400	-0.37201100
O	-0.74460800	-0.00006700	-0.14089200
H	-1.12240800	0.00046500	0.75568700

Table S*7*. Cartesian coordinates of optimized structure of **nh2o.** Calculations were performed at the PCM(H_2O)/BLYP-D3/6-311G(d,p) level of theory.

	x	y	z
N	-0.01632000	-0.55025400	0.00000000
H	0.12240000	-1.06028600	0.88036100
H	0.12240000	-1.06028600	-0.88036100
O	-0.01632000	0.74654400	0.00000000

Table S*8*. Cartesian coordinates of optimized structure of **nho.** Calculations were performed at the PCM(H_2O)/BLYP-D3/6-311G(d,p) level of theory.

	x	y	z
N	0.06360300	0.58904700	0.00000000
H	-0.95403800	0.93240900	0.00000000
O	0.06360300	-0.63196700	0.00000000

Table S*9*. Cartesian coordinates of optimized structure of **nh.** Calculations were performed at the PCM(H_2O)/BLYP-D3/6-311G(d,p) level of theory.

	x	y	z
N	0.00000000	0.00000000	0.13131500
H	0.00000000	0.00000000	-0.91920800

Table S*10*. Cartesian coordinates of optimized structure of **nhoh.** Calculations were performed at the PCM(H_2O)/BLYP-D3/6-311G(d,p) level of theory.

	x	y	z
N	0.72083500	-0.17824100	0.00001500
H	1.13723700	0.77292600	-0.00011300
O	-0.63714300	0.14927200	0.00001600
H	-1.08593400	-0.71941700	-0.00012100

Table S*11*. Cartesian coordinates of optimized structure of **no.** Calculations were performed at the PCM(H_2O)/BLYP-D3/6-311G(d,p) level of theory.

	x	y	z
N	0.00000000	0.00000000	-0.62129500
O	0.00000000	0.00000000	0.54363300

Table S*12*. Cartesian coordinates of optimized structure of **nh4.** Calculations were performed at the PCM(H_2O)/BLYP-D3/6-311G(d,p) level of theory.

	x	y	z
N	0.00000000	0.00000000	0.00000000
H	0.62084700	0.62084700	0.62084700
H	-0.62084700	-0.62084700	0.62084700
H	-0.62084700	0.62084700	-0.62084700
H	0.62084700	-0.62084700	-0.62084700

Table S*13*. Cartesian coordinates of optimized structure of **co2.** Calculations were performed at the PCM(H_2O)/BLYP-D3/6-311G(d,p) level of theory.

	x	y	z
C	0.00000000	0.00000000	0.00000000
O	0.00000000	0.00000000	1.17382700
O	0.00000000	0.00000000	-1.17382700

Table S*14*. Cartesian coordinates of optimized structure of **hcoo.** Calculations were performed at the PCM(H_2O)/BLYP-D3/6-311G(d,p) level of theory.

	x	y	z
C	0.00000000	0.00000000	0.44334300
H	0.00000000	0.00000000	1.54554800
O	0.00000000	1.05520300	-0.26285100
O	0.00000000	-1.05520300	-0.26285100

Table S*15*. Cartesian coordinates of optimized structure of **hcooh.** Calculations were performed at the PCM(H_2O)/BLYP-D3/6-311G(d,p) level of theory.

	x	y	z
C	-0.13067500	0.37270800	-0.00001900
O	1.06313900	-0.28612700	-0.00000800
O	-1.18478800	-0.22393900	0.00001100
H	1.79237000	0.36551500	0.00008600
H	-0.03512400	1.47876700	0.00000900

Table S*16*. Cartesian coordinates of optimized structure of **imin.** Calculations were performed at the PCM(H_2O)/BLYP-D3/6-311G(d,p) level of theory.

	x	y	z
C	-1.21366600	-0.14285600	0.00000500
H	-1.76516300	0.21690100	-0.88371600
H	-1.76566600	0.21816900	0.88292500
H	-1.20078100	-1.24047100	0.00075900
C	0.18993500	0.40820900	-0.00001400
H	0.26093800	1.51184100	0.00005100
N	1.21901300	-0.35832100	0.00001300
H	2.07996800	0.20969600	-0.00005300

Table S*17*. Cartesian coordinates of optimized structure of **imO.** Calculations were performed at the PCM(H_2O)/BLYP-D3/6-311G(d,p) level of theory.

	x	y	z
C	1.80843900	0.11709300	-0.00010800
H	2.37367200	-0.21672500	0.88481900
H	1.79140600	1.21645600	0.00094400
H	2.37337600	-0.21584900	-0.88544600
C	0.42559600	-0.46003600	0.00007600
H	0.24344500	-1.53412300	0.00009000
N	-0.65249100	0.29672100	0.00003100
H	-0.48263900	1.32205100	-0.00012900
O	-1.89200400	-0.07390000	-0.00003800

Table S*18*. Cartesian coordinates of optimized structure of **imH.** Calculations were performed at the PCM(H_2O)/BLYP-D3/6-311G(d,p) level of theory.

	x	y	z
C	1.26107500	-0.17693100	0.01649200
H	1.31949100	-1.06919900	-0.63251400

H	1.45509000	-0.53348100	1.05271300
H	2.09030500	0.48954800	-0.25990700
C	-0.05956600	0.52438500	-0.12702800
H	-0.13657900	1.57246800	0.17243800
N	-1.23104600	-0.23340300	0.11090600
H	-2.09784100	0.25023800	-0.12591000
H	-1.22219400	-1.16048100	-0.31994200

Table S*19*. Cartesian coordinates of optimized structure of **imOH_mH_bN.** Calculations were performed at the PCM(H_2O)/BLYP-D3/6-311G(d,p) level of theory.

	x	y	z
C	1.85755700	-0.09291900	-0.00014200
H	2.38750300	0.29153900	0.88561300
H	2.38809600	0.29405100	-0.88437800
H	1.91284800	-1.18890900	-0.00162600
C	0.42801600	0.37444400	0.00015200
H	0.21790600	1.45339800	0.00049800
N	-0.52982100	-0.48179700	0.00019300
O	-1.81096100	0.17673700	-0.00023800
H	-2.42335700	-0.58055100	0.00039400

Table S*20*. Cartesian coordinates of optimized structure of **nitren.** Calculations were performed at the PCM(H_2O)/BLYP-D3/6-311G(d,p) level of theory.

	x	y	z
C	1.14648300	-0.14438900	-0.00000500
H	1.15800400	-1.24020300	0.00030200
H	1.67334900	0.23281100	0.88851700
H	1.67319000	0.23229300	-0.88879900
C	-0.28667400	0.38831600	0.00000800
H	-0.38506300	1.49566000	-0.00003100
N	-1.32547600	-0.31201700	-0.00000100

Table S*21*. Cartesian coordinates of optimized structure of **h2.** Calculations were performed at the PCM(H_2O)/BLYP-D3/6-311G(d,p) level of theory.

	x	y	z
H	0.00000000	0.00000000	0.37423000
H	0.00000000	0.00000000	-0.37423000

Table S*22*. Cartesian coordinates of optimized structure of **im_mH_bC.** Calculations were performed at the PCM(H_2O)/BLYP-D3/6-311G(d,p) level of theory.

	x	y	z
C	-1.20330200	-0.16653100	0.00006400
H	-2.09569400	0.44618000	0.00008100
H	-1.30610600	-1.24586900	0.00008100
C	0.07287400	0.40761500	-0.00002000
H	0.12908700	1.50100400	-0.00004100
N	1.15313000	-0.34300300	-0.00004100

H	1.98336800	0.25320600	-0.00010000

Table S*23*. Cartesian coordinates of optimized structure of **imCO2_mH_bC.** Calculations were performed at the PCM(H_2O)/BLYP-D3/6-311G(d,p) level of theory.

	x	y	z
C	-2.04913000	0.54541900	0.28198500
H	-1.51302500	1.48985200	0.24507300
H	-3.09977200	0.53589700	0.56157900
C	-1.43501800	-0.64082000	-0.05057000
H	-2.01392100	-1.56324100	-0.10610200
N	-0.11144900	-0.79229100	-0.34342800
H	0.19339700	-1.73014300	-0.61397600
C	0.97796200	0.11845600	-0.04979400
O	0.82150300	1.32933700	-0.29279800
O	1.95982000	-0.49492000	0.44625900

[1] R. Car, M. Parrinello, *Phys. Rev. Lett*., **1985**, 55, 2471–2474.

[2] CPMD. Copyright IBM Corp, **1990–2008**; Copyright MPI für Festkörperforshung Stuttgart **1997–2001**. Available online: http://www.cpmd.org/ (accessed on 16 January 2012).

[3] D. A. Becke, *Phys. Rev. A*, **1988**, 38, 3098.

[4] C. Lee, W. Yang, R. G. Parr, *Phys. Rev. B*, **1988**, 37, 785-789.

[5] S. Grimme, *J. Comput. Chem.*, **2006**, 27, 1787–1799.

[6] N. Troullier, J. L. Martins, *Phys. Rev. B*, **1991**, 43, 1993–2006.

[7] M. Boero, M. Parrinello, K. Terakura, H. Weiss, *Mol. Phys*. **2002**, 100, 2935–2940.

[8] O. Gunnarsson, B. I. Lundqvist, *Phys. Rev. B*, **1976**, 13, 4274–4298.

[9] (a) D. A. Becke, *J. Chem. Phys*. **1993**, 98, 5648-5652. ; (b) S. Grimme, *J. Chem. Phys*. **2006**, 124, 034108.

[10] S. Grimme, *J. Chem. Phys*. **2006**, 124, 034108/1–16.

[11] C. Møller, M. S. Plesset, *Phys Rev*, **1934**, 46, 618.

[12] W. J. Hehre, L. Radom, P. v. R. Schleyer, J. A. Pople, *Ab Initio Molecular Orbital Theory*; Wiley, New York, **1986**.

[13] S. Miertus, E. Scrocco, J. Tomasi, *Chem Phys*, **1981**, 55,117– 129.

[14] Gaussian 16, Revision A.03, M. J. Frisch, G. W. Trucks, H. B. Schlegel, G. E. Scuseria, M. A. Robb, J. R. Cheeseman, G. Scalmani, V. Barone, G. A. Petersson, H. Nakatsuji, X. Li, M. Caricato, A. V. Marenich, J. Bloino, B. G. Janesko, R. Gomperts, B. Mennucci, H. P. Hratchian, J. V. Ortiz, A. F. Izmaylov, J. L. Sonnenberg, D. Williams-Young, F. Ding, F. Lipparini, F. Egidi, J. Goings, B. Peng, A. Petrone, T. Henderson, D. Ranasinghe, V. G. Zakrzewski, J. Gao, N. Rega, G. Zheng, W. Liang, M. Hada, M. Ehara, K. Toyota, R. Fukuda, J. Hasegawa, M. Ishida, T. Nakajima, Y. Honda, O. Kitao, H. Nakai, T. Vreven, K. Throssell, J. A. Montgomery, Jr., J. E. Peralta, F. Ogliaro, M. J. Bearpark, J. J. Heyd, E. N. Brothers, K. N. Kudin, V. N. Staroverov, T. A. Keith, R. Kobayashi, J. Normand, K. Raghavachari, A. P. Rendell, J. C. Burant, S. S. Iyengar, J. Tomasi, M. Cossi, J. M. Millam, M. Klene, C. Adamo, R. Cammi, J. W. Ochterski, R. L. Martin, K. Morokuma, O. Farkas, J. B. Foresman, and D. J. Fox, Gaussian, Inc., Wallingford CT, **2016**.